Journal of Nanobiotechnology

RESEARCH

Open Access

Recombinant high-density lipoprotein targeted delivery of celastrol to promote foam cells lipophagy against early atherosclerosis

Yang Li[1], Xiaoxia Xue[1], Liuchunyang Yu[1], Jinxiu Qian[1], Xiaoyu Li[1], Meng Tian[1], Jue Yang[1], Rongjun Deng[1], Cheng Lu[2*], Cheng Xiao[3*] and Yuanyan Liu[1*]

Abstract

Introduction Atherosclerosis serving as the main underlying factor of cardiovascular disease (CVD) remains the primary cause of mortality and morbidity globally, while the deposition of massive cholesterol in macrophage-derived foam cells exerts pivotal roles in the occurrence and progression of atherosclerosis. Celastrol (CEL) is a bioactive ingredient owning potent capability to modulate lipid metabolism, whereas the poor bioavailability and potential toxicity limit its clinical application.

Objectives This study aims to design a CEL-loaded recombinant high-density lipoprotein (rHDL) delivery platform for active targeting, which may effectively promote lipid degradation in foam cells and reversely transport excessive cholesterol to the liver for metabolism in time.

Methods The rHDL loaded with CEL (CEL-rHDL) was prepared by the thin film dispersion method. Then the anti-atherosclerotic efficacy and targeted delivery to foam cells of atherosclerotic lesions were verified both in vitro and in vivo. RNA-sequence was applied to reveal the potential mechanism against early atherosclerosis, which was further validated through several molecular biology experiments.

Results The prepared CEL-rHDL increased the targeting efficiency to foam cells of atherosclerotic lesions, mitigated its off-target toxicity, and improved anti-atherosclerotic efficacy. Importantly, CEL-rHDL decreased lipid storage in foam cells by triggering lipophagy via the activation of Ca^{2+}/CaMKKβ/AMPK/mTOR signaling pathway and reverse cholesterol transport (RCT).

Conclusion A combination of hypolipidemic chemo-intervention with rHDL participated specific and reverse delivery may offer a promising strategy for biocompatible treatment of early atherosclerosis.

*Correspondence:
Cheng Lu
lv_cheng0816@163.com
Cheng Xiao
xiaocheng@zryhyy.com.cn
Yuanyan Liu
yyliu_1980@163.com

Full list of author information is available at the end of the article

Graphical abstract

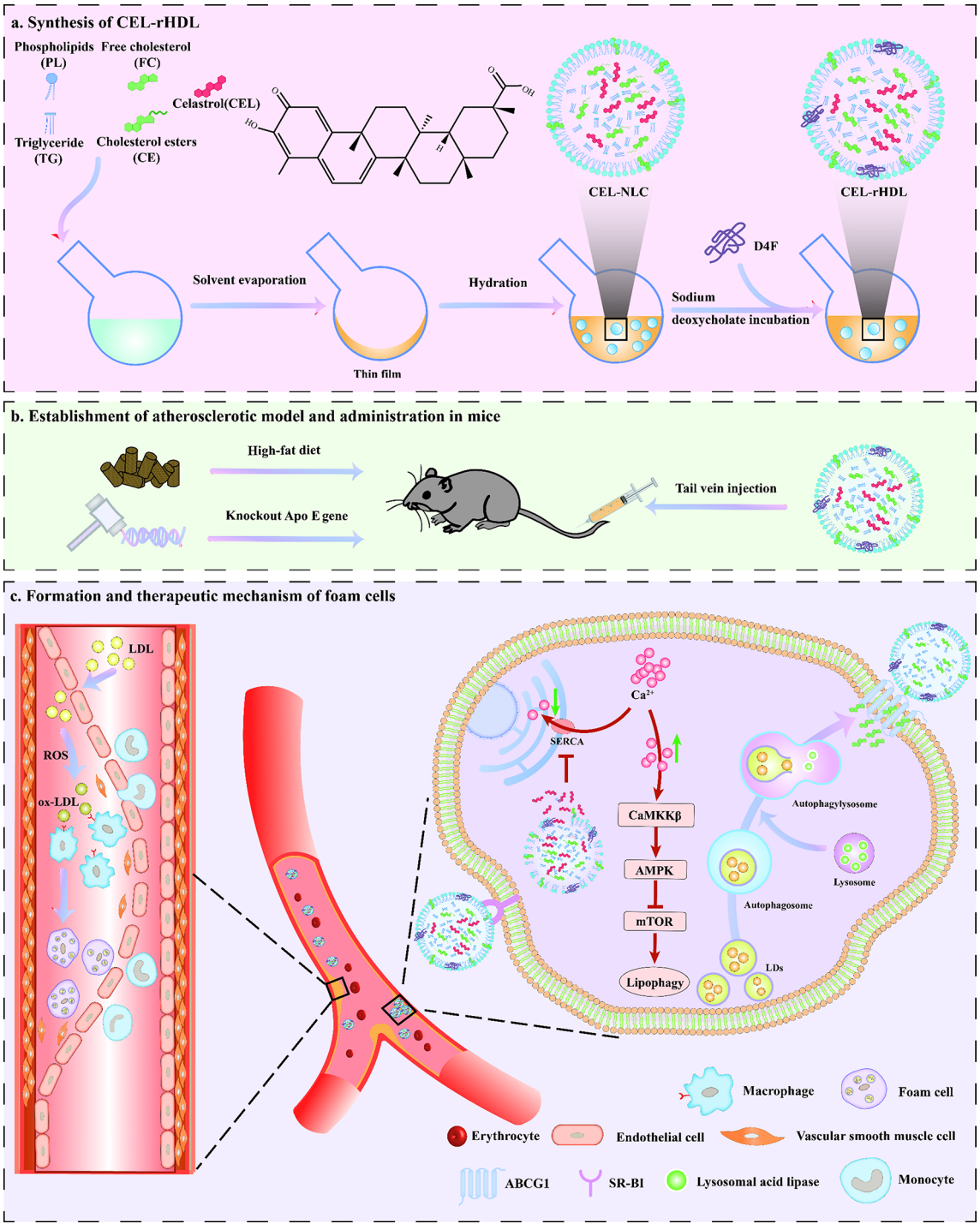

Keywords Atherosclerosis, Celastrol, rHDL, Targeted delivery, Lipophagy

Introduction

Atherosclerosis, a progressive inflammatory cardiovascular disease (CVD), is marked by the extensive accumulation of lipid-rich foam cells within the subendothelial regions of arterial walls. This condition is a major contributor to numerous severe vascular occurrences,

encompassing stroke, myocardial infarction and peripheral artery disease, thereby leading to significant morbidity and mortality globally [1, 2]. As the main components of atherosclerotic lesions, macrophage-derived foam cells act essential functions in the occurrence and development of inflammatory lesions and lipid homeostasis disruption [3]. During the initial phase of atherosclerosis, circulating monocytes penetrate into the subendothelial areas of impaired arteries and transform into activated macrophages, which subsequently recognize and unrestrictedly internalize oxidized low-density lipoprotein (ox-LDL) via surface scavenger receptors (SR) [4, 5]. When the absorption of ox-LDL exceeds the metabolic capacity of macrophages, the redundant cholesterol accumulates in cytoplasmic lipid droplets (LDs) in the form of cholesterol esters (CE), since then macrophages are transformed into foam cells, a sign of early atherosclerosis. The initial phase of atherosclerosis represents a crucial juncture for its advancement and reversal, especially as a key point for therapeutic intervention. Without timely intervention, the build-up of lipid-laden foam cells may exacerbate inflammatory process and contribute to the formation and rupture of unstable atherosclerotic plaques, increasing the risk of CVD, the stage with irreversible damage [6, 7]. Therefore, restraining macrophage-derived foam cells generation through restoring lipid homeostasis may be an effective way to alleviate the atherosclerotic progression.

Intriguingly, high-density lipoprotein (HDL) as a dynamic endogenous carrier to transport lipid, bears the capacity to accept excess free cholesterol (FC) from peripheral cells and motivate reverse cholesterol transport (RCT) in atherosclerotic protection. In addition, it can serve as a nano-carrier to transport diverse hydrophobic molecules to specific organs. It indicates that HDL is not only a carrier for safely targeted delivery of hydrophobic agents, but also a lipid carrier with therapeutic effect [8–10]. Endogenously derived HDL exists in two different forms including discoidal HDL and spherical HDL, the latter one is the dominant HDL form in circulation [11]. Spherical HDL owns a unique core-shell structure, consisting of a hydrophobic core composed of CE and triglyceride (TG) surrounded by a monolayer shell primarily made up of phospholipids (PL), FC and apolipoproteins (Apos) [12, 13]. As an active Apos component of HDL, apolipoprotein AI (Apo AI) comprises eight amphipathic α-helical domains and is crucial for maintaining the size and shape of natural HDL [14, 15]. Considering that isolating and purifying endogenous HDL from human serum is expensive and arduous, even exists the safety concerns of blood borne contamination, multiple Apo AI mimetic peptides have been developed for preparing recombinant HDL (rHDL) with similar properties to endogenous HDL as an alternative effective drug delivery platform [14, 16]. rHDL permits dual delivery of hydrophilic and hydrophobic molecules due to its amphiphilic nature. By imitating the shape and structure of endogenous HDL, rHDL could escape the clearance of mononuclear phagocyte system without triggering immunological responses, while also exhibiting complete biodegradability and excellent biocompatibility [17, 18]. Moreover, rHDL could improve the delivery of encapsulated cargo through targeting atherosclerotic lesion region to avoid off-target effects, for the possible mechanism of that rHDL with Apo AI is actively targeted to specific SR-BI receptor on foam cells [19]. Meanwhile, rHDL is as effective as native HDL in stimulating RCT to restrain the progression of atherosclerotic plaques [20, 21].

Here, rHDL is utilized to specifically deliver celastrol (CEL), a well-known hypolipidemic agent, to overcome its poor aqueous solubility, narrow therapeutic window, weak bioavailability and potential undesired side effects, which generate severe setback for its further clinical application [22]. CEL, a pharmacologically active pentacyclic triterpene, has recently been proved to possess potent lipid regulatory capabilities and promising therapeutic effects on lipid-related diseases, comprising atherosclerosis, obesity and non-alcoholic fatty liver disease (NAFLD) [23, 24]. Numerous evidence demonstrated that CEL could mitigate lipid metabolic disorders through modulating lipid profiles and pertinent metabolic processes, involving in the suppression of lipid synthesis, enhancement of lipid catabolism, blockade of intestinal absorption and facilitation of lipid transport [24–26].

The LDs serve as the primary location for CE storage within macrophage-derived foam cells, so increasing CE lipolysis in LDs may be an effective mechanism to alleviate the cholesterol burden within foam cells. In addition to the role of the cytoplasmic neutral CE hydrolases in CE metabolism, lipophagy has been shown to be an excellent regulatory mechanism to maintain lipid homeostasis [27–29]. Lipophagy, a special form of autophagy, selectively degrades CE stored in LDs via a lysosomal-dependent manner, contributing to regulate lipid metabolism and maintain cellular cholesterol homeostasis [30]. During the process of lipophagy, the membrane proteins of LDs are identified and sequestered by microtubule-associated protein 1 light chain 3II (LC3-II), forming double-membrane vesicles known as autophagosomes. These autophagosomes subsequently fuse with lysosomes to generate autolysosomes, where CE stored in LDs is hydrolyzed into FC through lysosomal acid lipase (LAL) [6]. Multiple studies have indicated that the promotion of lipophagy could facilitate cholesterol degradation and restrain foam cells formation, then mitigate the progression of atherosclerosis [29, 31, 32].

The present study aims to synthesize a CEL-loaded rHDL (CEL-rHDL) delivery platform with triple actions, including targeted delivery to the subendothelial foam cells, triggering lipophagic processes of foam cells and reverse transporting excessive cholesterol. Moreover, the potential molecular mechanism on how CEL-rHDL triggers lipophagy to reduce lipid accumulation in foam cells was discovered and verified, providing a novel biocompatible strategy for the precise treatment of early atherosclerosis (Fig. 1).

Materials and methods

Materials

CEL (over 98% purity) was acquired from bidepharm (Shanghai, China). Egg phospholipids and Glycerol trioleate were obtained from Solarbio (Beijing, China). D4F (an Apo AI mimetic peptide) was synthesized by SynthBio Co., Ltd (Hefei, China). Bovine serum albumin (BSA) and cholesterol were supplied from LABLEAD Biotechnology Co., Ltd (Beijing, China). Cholesteryl oleate was provided by aladdin (Shanghai, China). Human ox-LDL was derived from Yiyuan Biotechnologies (Guangzhou, China). Modified Oil Red O Stain kit and Fluo-4, AM were acquired from Beyotime Biotechnology (Shanghai, China). Dulbecco's modified Eagle medium (DMEM) was supplied by Thermo Fisher Scientific (Waltham, USA). Fetal bovine serum (FBS) was procured from Corning Co., Ltd (CA, USA). Penicillin-streptomycin was provided by Viva Cell Biosciences (Shanghai, China). Thapsigargin (TG), Compound C (CC), BAPTA/AM, STO-609, Bafilomycin A1 (Baf) and 3-Methyladenine (3-MA) were obtained from Topscience Co., Ltd (Shanghai, China). Rabbit antibodies against AMPK (5831), mTOR (2983), p-AMPK (2535), p-mTOR (5536) and P62 (5114) were supplied by Cell Signaling Technology (Beverly, MA, USA), rabbit antibody against LC3B (A19665) was supplied by ABclonal Biotech Co., Ltd (Wuhan, China), and rabbit antibodies against CaMKKβ (DF4793) and p-CaMKKβ (AF4487) were supplied by Affinity (Jiangsu, China). Coumarin 6 (C6) was provided by MedChemExpress (New Jersey, USA). 4% Rabbit red blood cells (RBCs) and NBD-cholesterol were supplied by Yuanye Bio-Technology Co., Ltd (Shanghai, China). 0.1% Triton X-100 was obtained from Macklin (Shanghai, China).

Preparation of CEL-rHDL

The preparation of CEL-rHDL was carried out through utilizing the thin film dispersion method, followed by sodium deoxycholate incubation, as previously outlined with minor modifications [1, 33, 34]. In brief, a lipid mixture containing 45 mg egg phospholipid, 15 mg glycerol trioleate, 20 mg cholesteryl oleate and 10 mg cholesterol was dissolved in 15 mL of methanol/chloroform solution (ratio volume 1:1) with the addition of 3.5 mg CEL. This mixture was then combined in an egg-plant flask and dried using a rotary evaporator (RE-52AA, Shanghai Yarong Biochemistry Instrument Factory, Shanghai, China) at a speed of 60 rpm under 45 ℃ to eliminate the organic solvent. Subsequently, 15 mL of 0.02 M Tris-HCl buffer (pH 8.0) comprising sodium deoxycholate was introduced into the flask, and the mixture was then rotated again for 1 h under 45 ℃. The obtained thin film was uniformly dispersed through vortex agitation for 15 min, followed by sonication (working for 5 s, resting for 5 s) for 5 min in an ice bath. After filtering through a 0.22 μm sterile filter, the CEL-nano lipid carrier (NLC) suspension was obtained. Next, 10 mL of CEL-NLC suspension was incubated with an equal volume of Tris-HCl buffer comprising D4F (5 mg) at a speed of 600 rpm for 8 h. To remove free CEL and sodium deoxycholate, the samples were dialyzed in a 10 kDa dialysis bag (Solarbio, Shanghai, China) for 48 h. Consequently, CEL-rHDL suspension was obtained, and CEL-NLC and CEL-rHDL suspension were freeze-dried overnight.

In vitro characterizations

Mean size and zeta potential

The measurements of the mean sizes and zeta potentials for CEL-NLC and CEL-rHDL preparations were conducted using a dynamic light scattering (DLS) analyzer (Zetasizer Nano ZS90, Malvern, UK). Prior to analysis, all samples were appropriately diluted with ddH_2O and each measurement was replicated three times to ensure accuracy and consistency.

Encapsulation efficiency (EE%) and drug loading efficiency (DL%)

Samples of 5 mg lyophilized CEL-NLC and CEL-rHDL were redissolved in methanol and demulsified by ultrasound. The EE and DL of CEL-NLC and CEL-rHDL were analyzed using an UPLC method employing the Waters ACQUITY UPLC H-Class system. Operating at a wavelength of 425 nm, the system utilized an RP18 column maintained at a controlled temperature of 35 ℃. The mobile phase comprised methanol and 1% HAC, with a volume ratio of 90:10. The flow rate was maintained at a consistent speed of 0.3 mL/min throughout the analysis. The measurements were performed in triplicate. EE and DL were calculated as follows:

$$EE\ (\%) = \frac{mass\ of\ loaded\ CEL}{total\ amount\ of\ CEL} \times\ 100\%$$

$$DL\ (\%) = \frac{mass\ of\ loaded\ CEL}{mass\ of\ CEL - rHDL} \times\ 100\%$$

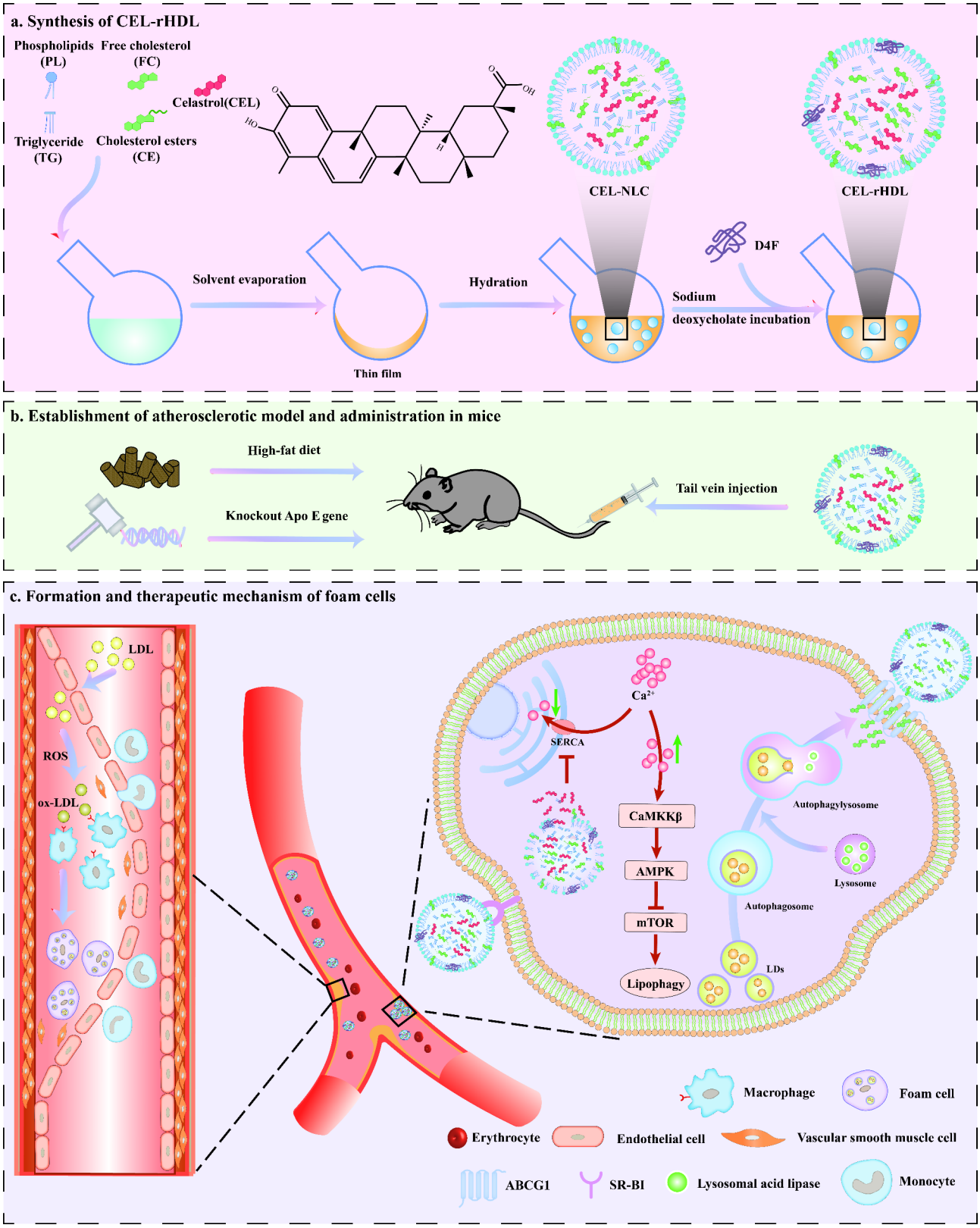

Fig. 1 Schematics depicting the synthesis of CEL-rHDL, establishment of atherosclerotic model and administration in mice, as well as the formation and therapeutic mechanism of foam cells (Schematic Figures are designed by Adobe Illustrator)

Morphology

CEL-NLC and CEL-rHDL were diluted accordingly, and individual droplet of each sample was added to the surface of the carbon-coated copper grid, which was placed onto a filter paper within a clean surface dish. A drop of 2% phosphotungstic acid solution was then introduced to the surface dish and the carbon-coated copper grid was inverted on the phosphotungstic acid drop with tweezers for 3–5 min, followed by complete drying at room temperature. The morphologies of CEL-NLC and CEL-rHDL were individually visualized through the use of transmission electron microscopy (TEM, JEM-1400Flash, JEOL, JPN).

In vitro release study

CEL release profiles from CEL-rHDL were evaluated in phosphate buffered saline (PBS) at pH values of 5.5 and 7.4 [35]. In brief, 2 mL of CEL-rHDL was placed in a 10 kDa dialysis bag, followed by incubation in 200 mL of an appropriate release buffer at 37 ℃ for 72 h under 100 rpm stirring. 0.5 mL of release buffer was collected at 1, 2, 4, 8, 12, 24, 36, 48, 60 and 72 h, as well as replaced with an equivalent volume of fresh PBS solution. The CEL content in separated supernatant samples was conducted through UPLC.

Serum stability assays

The stability of CEL-rHDL was examined under conditions of FBS exposure. Specifically, an equal volume of FBS was mixed with CEL-rHDL and incubated at 37 ℃ for 1, 6, 12 and 24 h. The samples were then diluted 50-fold with ddH_2O [36]. The particle size distribution and zeta potential of CEL-rHDL were detected through the DLS Analyzer.

Hemolysis

For hemolysis evaluation, CEL-rHDL samples with concentrations ranging from 3 to 48 μg/mL were prepared. These samples were mixed with 4% RBCs suspension (a volume ratio of 4:1) in the tube. Deionized water served as the positive control and PBS served as the negative control. All samples were incubated with 4% RBCs suspension for 2 h, followed by centrifugation at 2500 rpm for 5 min. The hemoglobinic absorbance in the supernatant was determined at 545 nm by enzyme-labeled instrument. The calculation of the hemolysis rate proceeded as follows: hemolysis (%) = $(A_S - A_{C-})/(A_{C+} - A_{C-})$. A_S, A_{C-} and A_{C+} represented hemoglobinic absorbance of the sample groups, negative control and positive control group, respectively [35].

Cell culture

Currently, U937, THP-1 and RAW264.7 cells are commonly utilized in the establishment of foam cell models. Among these cells, RAW264.7 cells exhibit stability, ease of culturability and strong adherence properties. Consequently, RAW264.7 cells have been extensively employed in numerous studies to investigate the formation pathway of foam cells [37].

RAW264.7 cells were procured from Fenghui Biotechnology Co., Ltd (Hunan, China). The cells were incubated in complete DMEM comprising 1% penicillin-streptomycin and 10% FBS, and the incubation conditions were set at 37 ℃ in a humidified incubator with 5% CO_2. For experimental purposes, RAW264.7 cells were planted into 6-well plates and incubated overnight. Subsequently, RAW264.7 cells were induced to differentiate into foam cells after incubation with 80 μg/mL of ox-LDL for 24 h.

Cell viability analysis

RAW264.7 cells were seeded into 96-well plates and each well was incubated with 100 μL of complete medium for overnight incubation. After constructing foam cells model, the concentration of CEL and CEL-rHDL (CEL concentration in CEL-rHDL) in each well was 0, 0.2, 0.4, 0.5, 0.6, 0.7, 0.8, 1.0, 2.0, 4.0 μM, with triplicate wells for each concentration. After the samples culturing for 24 h, 10 μL of 10% CCK8 working solution was then introduced to each well. Following incubation for 1–2 h in a cell incubator, the 96-well plates were placed in an enzyme-labeled instrument with a wavelength of 450 nm to detect the absorbance of each well. The data was recorded and analyzed by GraphPad Prism 9.0.

Cellular uptake of CEL-rHDL

To ascertain the targeting property of SR-BI, C6 served as a hydrophobic fluorescent probe to indicate the localization of CEL, which was integrated into rHDL. The uptake of C6-rHDL was observed by confocal laser scanning microscopy (CLSM, Leica TCS SP8, Germany). RAW264.7 cells were plated into confocal dishes and incubated with ox-LDL to induce foam cells formation. Next, the culture medium was substituted by 0.5 mL of fresh medium devoid of FBS including C6-NLC and C6-rHDL. For the competition assay, an excess of free D4F was introduced 2 h prior to the addition of C6-rHDL. Following incubation for 4 h, the culture medium was poured off, as well as foam cells were rinsed thrice with PBS and then fixed with 4% paraformaldehyde for 15 min. Finally, DAPI was introduced to stain the cell nucleus. CLSM observations were conducted with excitation wavelengths of 465 nm and 359 nm, and emission wavelengths of 502 nm and 461 nm for C6 and DAPI, respectively [36].

Determination of lipid

The Oil Red O was used to stain the intracellular lipid (Beyotime Biotechnology Co., Ltd, Shanghai, China).

Briefly, RAW264.7 cells were exposed to ox-LDL to induce foam cell formation. After treating with or without CEL and CEL-rHDL, cells were rinsed thrice with PBS and fixed with 4% paraformaldehyde (LABLEAD Biotechnology Co., Ltd, Beijing, China) for 10 min at 25 ℃. Then cells were stained with Oil Red O for 0.5 h and observed under an inverted fluorescence microscope (IX73, Olympus, Tokyo, Japan) after washing. As well, the CE content was measured by total cholesterol (TC) and FC content assay kit (Solarbio, Beijing, China) and the calculation formula was as follows:

$CE\% = (TC - FC)/TC \times 100\%$.

Autophagic flux analysis

RAW264.7 cells were seeded onto confocal dishes and transfected with mCherry-GFP-LC3 adenovirus (HanBio Technology Co. Ltd., Shanghai, China). RAW264.7 cells were incubated with adenovirus for 24 h in the medium, followed by the removal of the adenovirus. Subsequently, the cells were triggered to differentiate into foam cells through incubating with ox-LDL for 24 h. After this treatment, CEL and CEL-rHDL were added to foam cells and cultured for a further 24 h. For experiments designed to investigate the effect of autophagy inhibition, foam cells were pretreated with either 3-MA or Baf prior to the addition of CEL and CEL-rHDL. Finally, autophagy flux was visualized and analyzed using a confocal laser scanning microscope.

Measurement of intracellular free calcium

The intracellular calcium levels were quantitatively determined through the utilization of the Fluo-4, AM dye. In brief, RAW264.7 cells were seeded in 6-well plates and cultured with ox-LDL to stimulate foam cells generation. Foam cells were rinsed twice with PBS following exposure to 0.8 μM CEL and CEL-rHDL for 4 h. The cell suspensions were then cultured with 5 μM Fluo-4, AM for 0.5 h under dark conditions. After incubation, foam cells were rinsed with PBS and fluorescence intensity was observed under inverted fluorescence microscope [38].

Cholesterol efflux assay

RAW264.7 cells were seeded in 6-well plates and cultured with ox-LDL to stimulate foam cells formation. Then foam cells were cultured in a serum-free medium containing 5.0 μmol/L NBD-cholesterol and 0.2% BSA for 24 h to allow NBD-cholesterol labeling. Following the labeling period, the cells were rinsed thrice with PBS. Thereafter, CEL, CEL-rHDL and rHDL were introduced to initiate cholesterol efflux for 6 h. After incubation, the culture medium was gathered and intracellular cholesterol was extracted by lysing foam cells with 0.1% Triton X-100 for measuring fluorescence intensity (FI). The quantification of FI within both the culture medium and cell lysate was conducted via a microplate reader setting at 469 nm excitation and 537 nm emission. The percentage of NBD-cholesterol efflux was determined through the following formula: NBD-cholesterol efflux% = (medium FI)/(medium FI + intracellular FI) × 100% [39].

RNA-seq

RAW264.7 cells were seeded in six-well plates and cultured with ox-LDL to trigger foam cells generation. Next, the foam cells were incubated with either 0.8 μM CEL or CEL-rHDL for another 24 h. The TRIzol reagent (Invitrogen, CA, USA) was used to extract total RNA, which was assessed via Agilent 2100 BioAnalyzer (Agilent Technologies, CA, USA) and NanoDrop spectrophotometer (Thermo Scientific, DE, USA). The libraries for sequencing were constructed by the NEBNext® Ultra™ RNA Library Prep Kit for Illumina® (NEB, USA), and sequenced on the Illumina Novaseq 6000 platform of Beijing Allwegene Technology Company Limited (Beijing, China), as well as paired-end 150 bp reads were generated. Prior to downstream analysis, the raw sequencing data underwent initial processing to obtain high-quality clean data through the elimination of reads containing adapters, poly-N sequences and those with low quality. These clean reads were then mapped to the reference genome sequence by STAR.

Quantitative Real-Time PCR (qPCR) analysis

The FastPure Cell/Tissue Total RNA Isolation Kit V2 (Vazyme Biotech) was used to extract samples RNA and the ABScript III RT Master Mix for qPCR with gDNA Remover (Abclonal, RK20429) was used for synthesizing cDNA. As well, qPCR was performed by 2 × Universal SYBR Green Fast qPCR Mix (Abclonal, RK21203). All primers used in qPCR were synthesized by Sangon Biotech Co., Ltd (Shanghai, China). After designing the primer sequences using Primer BLAST, their validity was confirmed by Oligonucleotide Properties Calculator. The resulting primer sequences are presented below: CaMKKβ, forward ACGCTGTACTGCTTTGTCTTTGG, and reverse ATATCGGGCTGGTCGGGAAAC; AMPK, forward GAGTGTTCGGAGGAGGAGGTC and reverse CTGTTGTCTATGATGAGGTGGTAGG; mTOR, forward ACCGTCCGCCTTCACAGATAC and reverse CGTTCCTTCTCCTTCTTGACACAG; LC3, forward: CGTCCTGGACAAGACCAAGT and reverse ATTGCTGTCCCGAATGTCTC; SQSTM1/P62, forward GCTGCCCTATACCCACATCT and reverse CGCCTTCATCCGAGAAAC; GAPDH, forward ACGGCAAATTCAACGGCACAG and reverse ACACCAGTAGACTCCACGACATAC. The 2-ΔΔCt method was employed to assess the relative mRNA levels of each gene.

Western blot analysis

To extract total protein, RAW264.7 cells were firstly planted into a six-well plate and induced foam cells generation. Next, foam cells were incubated with either 0.8 μM CEL or CEL-rHDL for another 24 h. The lysis buffer was used to extract the total protein and the quantification of the total protein concentration was achieved through a bicinchoninic acid (BCA) kit (Beyotime Biotechnology, Shanghai, China). The 20 μg total protein of each sample was loaded onto SDS-PAGE gel for electrophoretic separation. The separated proteins were then transferred onto a membrane and blocked with 5% nonfat milk. The membrane was incubated overnight at 4 ℃ with specific primary antibodies against β-actin, CaMKKβ, p-CaMKKβ, AMPK, mTOR, p-AMPK, p-mTOR, LC3B and P62. After incubating with secondary antibodies for 1 h, the membrane was visualized using an ECL reagent (E1050, Lablead) and exposed to the Bio-Rad Chemi Doc touch imaging system.

Animals, treatments and in vivo distribution

Eight-week-old male Apo $E^{-/-}$ C57BL/6 mice, normal diet and high-fat diet (comprising 78.85% basic forage, 0.15% cholesterol and 21% fat) were acquired from SiPeiFu Biotechnology Co., Ltd (Beijing, China). The mice were randomly fell into 4 groups ($n=6$) involving the control group, model group, CEL group and CEL-rHDL group. Mice in the control group were fed a normal diet for 8 weeks, while mice in the other 3 groups were fed a high-fat diet for 8 weeks. In the CEL group and CEL-rHDL group, six time nodes (5 min, 0.5 h, 2 h, 8 h 16 h and 24 h) were selected for blood collection to measure plasma CEL concentration, and the results indicated that CEL-rHDL reached its peak immediately and then gradually declined to a low level approximately 24 h after a single intravenous administration, which is in line with literature [1, 34]. After 4 weeks of feeding, mice in the CEL group and CEL-rHDL group were injected with CEL (2 $mg.kg^{-1}.d^{-1}$) and CEL-rHDL (CEL content of 2 $mg.kg^{-1}.d^{-1}$) through the tail vein for 4 weeks, as well as mice in the control group and model group were injected with an equivalent dose of normal saline.

For the in vivo distribution assay, DiR (MedChemExpress, New Jersey, USA) was loaded into CEL-NLC and CEL-rHDL referring to 2.2. To demonstrate the plaque targeting properties of CEL-rHDL, the Apo $E^{-/-}$ atherosclerotic mice were classified into 3 groups containing free DiR, CEL-NLC/DiR and CEL-rHDL/DiR, and DiR (1 mg/kg) was administrated through the tail vein [40]. After 12 h administration, the mice were sacrificed to obtain aortic tree and imaged using a small animal imaging system (Perkin Elmer, America).

Biochemical serum analysis

After the end of treatment with CEL and CEL-rHDL, blood samples from mice were obtained using eyeball blood collection for serum preparation. Blood urea nitrogen (BUN), Alanine aminotransferase (ALT), aspartate transaminase (AST), LDL-cholesterol (LDL-C), TC, TG and HDL-cholesterol (HDL-C) were quantitatively assayed through the automatic biochemical analyzer (Mindray, BS-240 Vet, China).

Detection of atherosclerotic lesions in full-length Aorta, aortic arches and aortic roots

After blood collection, mice were anesthetized and dissected. Atherosclerotic lesions in various areas of experimental mice were treated, imaged and quantitatively analyzed. Aortic arch lesions were photographed against a blue background immediately following perfusion. Next, the heart along with the entire aorta (containing aortic arch, thoracic aorta and abdominal aorta) was taken from mice and divided into the aortic part and heart part, which were used to image the atherosclerotic lesions of the entire aorta and aortic root respectively. The aorta segment was fixed with 4% paraformaldehyde, cut lengthwise, stained with Oil Red O and photographed [34]. The heart part was dehydrated with ethanol, transparent, impregnated with wax, rapidly frozen, sliced (thickness about 10 μm), stained with hematoxylin-Oil Red and photographed. ImageJ software was used for image processing and quantitative analysis.

Safety evaluation of CEL-rHDL

Assessing the potential toxicity of drugs in vivo is crucial for their safe and effective use. To determine the toxicity of CEL-rHDL and CEL, the histological analysis was conducted on vital organs from Apo $E^{-/-}$ mice. Briefly, the liver, heart, spleen, kidney and lung tissue of treated mice were collected for H&E staining to visualize tissue morphology, and photographs were taken using a light microscope for further pathological analysis.

Ethics statement

All experiments concerning animals in this study were rigorously conducted in accordance with the relevant laws and regulations on the welfare and ethics of experimental animals (Approval NO. JLHK-20230831-01).

Statistical analysis

All available data presented were derived from at least three independent experiments and were presented as mean ± standard deviation (SD). GraphPad Prism 9.0 software was utilized for statistical analysis. Unpaired t-tests or one-way ANOVA was applied to compare groups. P-value less than 0.05 was deemed statistically

significant ($^{*}P < 0.05$, $^{**}P < 0.01$, $^{***}P < 0.001$ and $^{****}P < 0.0001$).

Results

Characterization of CEL-rHDL

CEL-rHDL was prepared by the thin film hydration method and CEL was encapsulated into the hydrophobic core of rHDL, which was subjected to surface modification with D4F to promote targeting. TEM imaging showed uniform size of spherical CEL-NLC and CEL-rHDL, consistent with detective results by Malvern ZetaSizer (Fig. 2B). Table 1 detailed the physicochemical characteristics of CEL-NLC and CEL-rHDL. The mean size of CEL-NLC and CEL-rHDL were 110.47 ± 4.54 nm and 132.83 ± 0.72 nm respectively. The mean size of prepared CEL-rHDL was slightly larger than CEL-NLC, likely attributed to the surface D4F modification. The Zeta potential was − 58.53 ± 0.96 mV for CEL-NLC and − 47.8 ± 0.78 mV for CEL-rHDL, and the reduction of the potential of CEL-rHDL was due to the positive charge of D4F (Fig. 2C). The EE% and DL% of CEL-NLC and CEL-rHDL were 60.24 ± 3.59% and 2.21 ± 0.05% vs. 81.53 ± 1.26% and 3.02 ± 0.01%, respectively.

In vitro drug release study

In neutral (pH 7.4) PBS, 24.33 ± 2.03% of encapsulated CEL was released, while in acidic (pH 5.5) PBS, CEL-rHDL released 61.67 ± 2.08% of CEL (Fig. 2D). As an Apo AI mimetic peptide, D4F owns a role similar to that of Apo AI in stabilizing CEL-rHDL structure under neutral conditions. Whereas, the acidic environment could alter the structure and function of D4F, diminishing its ability to stabilize CEL-rHDL and leading to greater drug release under an acidic environment. Atherosclerotic lesions generally cause a local acidic extracellular microenvironment [12]. This pH-responsive drug release behavior may strengthen drug release within atherosclerotic plaques. Given the above promising properties, CEL-rHDL was considered to be a viable drug delivery tool worthy of further experimental investigation.

Serum stability assays of CEL-rHDL

The size changes of CEL-rHDL were used as stability indexes in the presence of FBS in vitro. As depicted in Fig. 2E, the particle size of CEL-rHDL showed no significant changes during incubation with FBS for 24 h and the PDI was less than 0.3. The variations of zeta potential were also limited (Fig. 2F), the fluctuation of zeta potential could be explained that nano-particles dynamically moved during the experiment, before 12 h, they tended to slight aggregation movement possibly by association with proteins present in FBS, which also led to mildly lowering in the surface charge [41, 42]. While, after 12 h, they tended to adverse movement. The results indicated that CEL-rHDL owned sufficient stability in the plasma and rHDL could be used as a stable system delivery tool for CEL.

Blood compatibility of CEL-rHDL

To evaluate the safety of intravenously injecting CEL-rHDL, a hemolysis test was performed to assess its blood compatibility. As shown in Fig. 2G, although the hemolysis rate gradually increased with the CEL-rHDL concentration increasing from 3 to 48 μg/mL, the hemolysis rate of all samples was less than 5%. The results demonstrated that CEL-rHDL exhibited satisfactory biocompatibility and the safety of intravenous injection.

CEL-rHDL reduces lipid accumulation in foam cells

RAW264.7 cells were cultured with ox-LDL to build foam cells model. Firstly, the effect of various concentrations of ox-LDL on macrophages activity was investigated and the result suggested that ox-LDL had little effect on macrophages activity in concentrations range from 0 to 120 μg/mL (Fig. 3A). Then, to detect the effect of ox-LDL at different concentrations on intracellular lipids, Oil Red O staining was employed to visualize the lipids within RAW264.7 cells following incubation with ox-LDL, as well as intracellular CE was quantified by TC and FC detection kits. The LDs gradually increased with the elevation of ox-LDL concentration and CE content exceeded 50% with ox-LDL concentration of not less than 80 μg/mL (Fig. 3D, F-L). Based on this, RAW264.7 cells were cultured with 80 μg/mL ox-LDL for 24 h to generate foam cells in subsequent experiments.

After that, the effect of CEL and CEL-rHDL on the viability of foam cells was studied. As depicted in Fig. 3B, C, foam cells viability decreased significantly at concentrations exceeding 0.8 μM. Therefore, 0.8 μM was administered as the dosage of CEL and CEL-rHDL in subsequent cell experiments. Oil Red O staining indicated that CEL and CEL-rHDL could effectively decrease lipid accumulation in foam cells, and the effect of CEL-rHDL was superior to CEL (Fig. 3M, N). Moreover, the CE content in foam cells model was 54.41%, which decreased to 40.76% and 30.81% after treatment with CEL (0.8 μM) and CEL-rHDL (CEL content of 0.8 μM), respectively (Fig. 3E). These findings show that CEL-rHDL may act a crucial function in lipid metabolism.

Intracellular uptake of CEL-rHDL for SR-BI targeting

SR-BI is an integral membrane protein overexpressed in foam cells of atherosclerotic lesions that can be specifically recognized by D4F on the surface of CEL-rHDL for targeted delivery. Hydrophobic fluorescence dyes C6 was utilized as a substitute for CEL and incorporated into rHDL, as well as the cellular uptake of C6-rHDL was analyzed via CLSM. As shown in Fig. 4A, the fluorescence

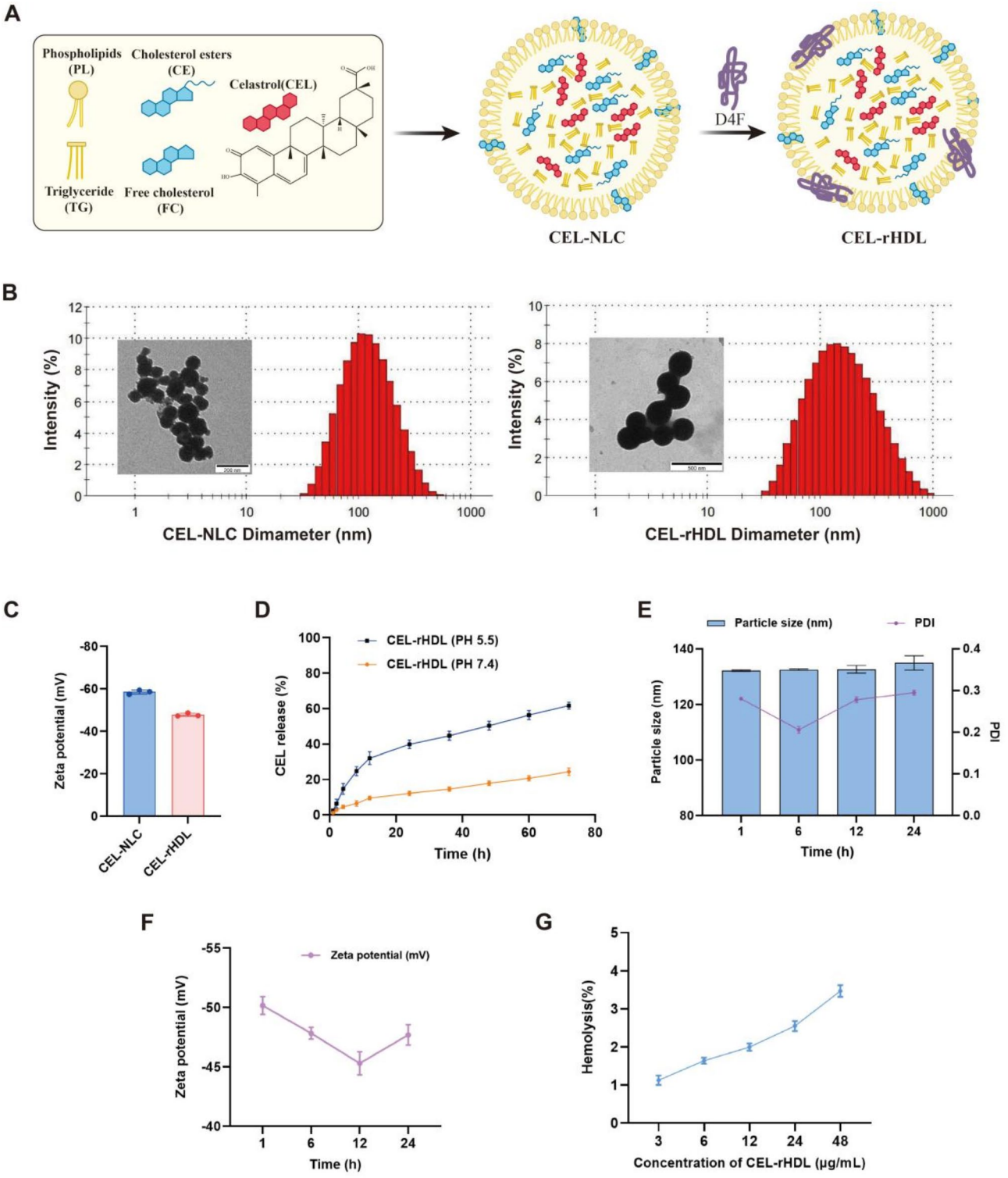

Fig. 2 The characterization, drug release profile, stability and hemocompatibility of CEL-rHDL. (**A**) Schematic diagram of CEL-rHDL. (**B**) TEM images and size distributions of CEL-NLC and CEL-rHDL. (**C**) Zeta potential of CEL-NLC and CEL-rHDL. (**D**) CEL release from CEL-rHDL in PBS at different pH. (**E**) The particle size and PDI changes of CEL-rHDL in FBS. (**F**) Zeta potential changes of CEL-rHDL in FBS. (**G**) Hemolysis rate at different concentration of CEL-rHDL

Table 1 The mean size, zeta potential, PDI, EE and DL of CEL-NLC and CEL-rHDL (mean ± SD, $n = 3$)

	CEL-NLC	CEL-rHDL
mean size (nm)	110.47 ± 4.54	132.83 ± 0.72
zeta potential (mV)	-58.53 ± 0.96	-47.8 ± 0.78
polydispersity index (PDI)	0.233 ± 0.004	0.289 ± 0.009
EE (%)	60.24 ± 3.59	81.53 ± 1.26
DL (%)	2.21 ± 0.05	3.02 ± 0.01

intensity of C6-rHDL in foam cells was stronger than that of C6-NLC without D4F modification, confirming that C6-rHDL possessed larger cellular uptake ascribed to the active targeting capacity of D4F on the surface of C6-rHDL for SR-BI [43]. Meanwhile, the uptake of C6-rHDL pretreated with excess free D4F was also provided. Compared with C6-rHDL, the uptake of C6-rHDL was significantly weakened in foam cells pretreated with excess free D4F due to competitively consume SR-BI, further demonstrating that the interaction between D4F and SR-BI may heighten atherosclerotic lesions targeting capacity of CEL-rHDL.

Effect of CEL-rHDL on autophagy flux in foam cells

A large amount of LDs in the cytoplasm is a feature of macrophage-derived foam cells, so promoting CE lipolysis of LDs may be an effective strategy to sustain lipid homeostasis in foam cells. In addition to the role of cytoplasmic CE hydrolases in CE metabolism, lipophagy has been proved to degrade LDs in an LAL-dependent manner, refraining cytoplasmic lipid deposition and exhibiting protective effect against atherosclerosis [44]. Noticeably, the above experiments have confirmed that CEL-rHDL possesses potent lipid-lowering ability in foam cells, and we speculate that this effect of CEL-rHDL is achieved by facilitating the lipophagic process of foam cells.

Next, to further verify the effect of CEL-rHDL on autophagy flux in foam cells, mCherry-GFP-LC3B adenovirus were applied to transfect cells and confocal images were obtained. During the process of autophagy, autophagosomes showed yellow spots due to both mCherry (a red fluorescent protein, RFP) and GFP (a green fluorescent protein) fluorescence [45]. GFP fluorescence is sensitive to acidic environment and it is quenched after the fusion of autophagosome with lysosome to form autolysosomes, whereas RFP fluorescence could be retained due to its stability [46]. Thus, changes in intracellular autophagic flux could be assessed by the ratio of GFP to RFP spots [47]. In comparison with the control group, the ratio of GFP to RFP was decreased after treatment with CEL and CEL-rHDL, indicating a relative increase in autophagy flux. As well, the autophagy flux induced by CEL-rHDL group was superior to CEL group (Fig. 5A).

Autophagy inhibitor restrains the lipophagy-promoting effect of CEL-rHDL

These experiments indicated that CEL-rHDL could facilitate lipophagy and lessen lipid deposition in foam cells. To confirm whether lipid degradation is mediated through lipophagy induction, 3-MA and Baf, two autophagy inhibitors, were applied to observe lipid accumulation and autophagy-related proteins expression in foam cells. 3-MA could suppress autophagosomes generation, while Baf restrains autolysosome formation via interrupting the fusion of autophagosomes and lysosomes [47]. In the presence of 3-MA or Baf, LDs and CE were prominently heightened in CEL and CEL-rHDL-treated foam cells (Fig. 6), suggesting that autophagy inhibitors mitigated the role of CEL-rHDL in lipid degradation in foam cells. The mCherry-GFP-LC3B adenovirus was employed to track autophagy flux to further verify the function of autophagy inhibitors. As shown in Fig. 7A, combining 3-MA or Baf with either CEL or CEL-rHDL in foam cells significantly heightened the proportion of green and red spots compared to treatment CEL or CEL-rHDL alone, suggesting that autophagy inhibitors interfered with the process of lipophagy. Furthermore, pretreatment with 3-MA increased P62 level and decreased LC3-II/LC3-I expression ratio, while P62 level and LC3-II/LC3-I expression ratio were increased in the presence of Baf (Fig. 7C). The above experimental data demonstrated that the effects of CEL and CEL-rHDL on lipid metabolism in foam cells were reversed by autophagy inhibitors.

RNA-seq analysis

The above Oil Red O staining and CE quantitative test data indicated that CEL-rHDL exhibited much superior hypolipidemic effects on foam cells than free CEL. In order to better explore the underlying hypolipidemic mechanism, whole genome RNA-sequencing was carefully performed on foam cells treated with CEL and CEL-rHDL to investigate the relevant molecular biological processes and signaling pathways. Correlation analysis indicated a strong relevance among the experimental replicates within each treatment group (Fig. 8A). The clustering analysis of DEGs also revealed the expected inter-sample relationship (Fig. 8B). Compared to the control group, the CEL group exhibited 4486 differential expressed genes (DEGs), including 2259 genes upregulated and 2227 genes downregulated. While the CEL-rHDL group displayed 5143 DEGs relative to the control group, with 2622 genes upregulated and 2521 genes downregulated. Compared to the CEL group, the CEL-rHDL group showed 850 DEGs, of which 452 genes were upregulated and 398 genes were downregulated (Fig. 8C). In terms of biological processes, DEGs were mainly associated with metabolic processes, including organic substance metabolic process, cellular metabolic process,

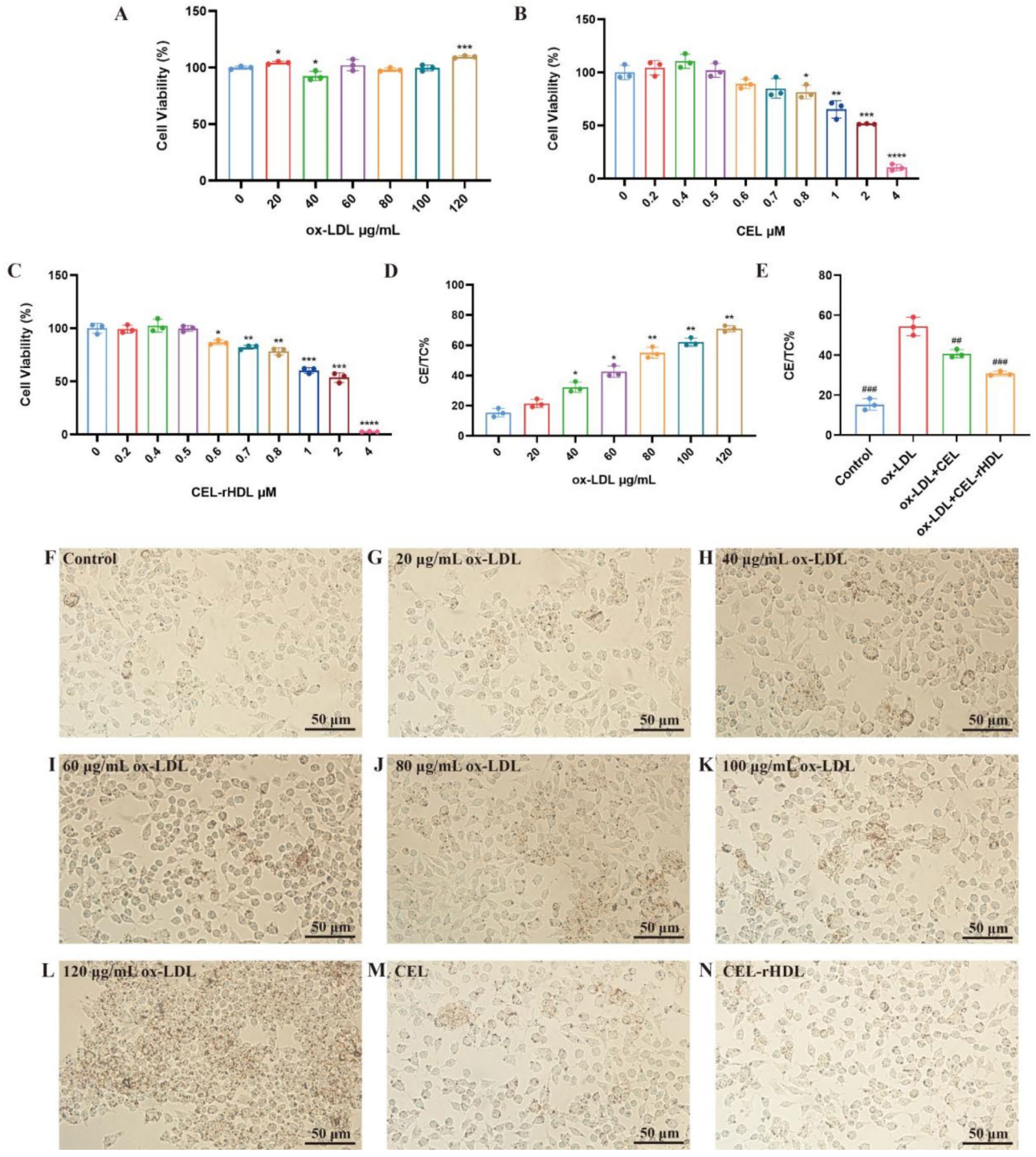

Fig. 3 Ox-LDL induces foam cells formation while CEL and CEL-rHDL decreases lipid deposition in foam cells. (**A**) The cell viability of RAW264.7 cells after incubation with ox-LDL. (**B**-**C**) The cell viability of foam cells after incubation with CEL and CEL-rHDL for 24 h. (**D**) The quantification of CE at different concentrations of ox-LDL. (**E**) The CE quantification in foam cells after CEL (0.8 μM) and CEL-rHDL (CEL content of 0.8 μM) treatment. (**F**-**N**) Oil Red O staining (scale bar: 50 μm). *$p < 0.05$, **$p < 0.01$, ***$p < 0.001$ and ****$p < 0.0001$ vs. 0 μg/mL; #$p < 0.05$, ##$p < 0.01$ and ###$p < 0.001$ vs. ox-LDL

primary metabolic process and cellular macromolecular metabolic process, suggesting that CEL-rHDL was involved in regulating multiple aspects of atherosclerosis (Fig. 8D). Cell cycle and lipophagy are both indispensable components of cell life activities, and the intricate interactions between them are of great significance for maintaining cellular homeostasis and responding to changes in the external environment [48–50]. Studies have

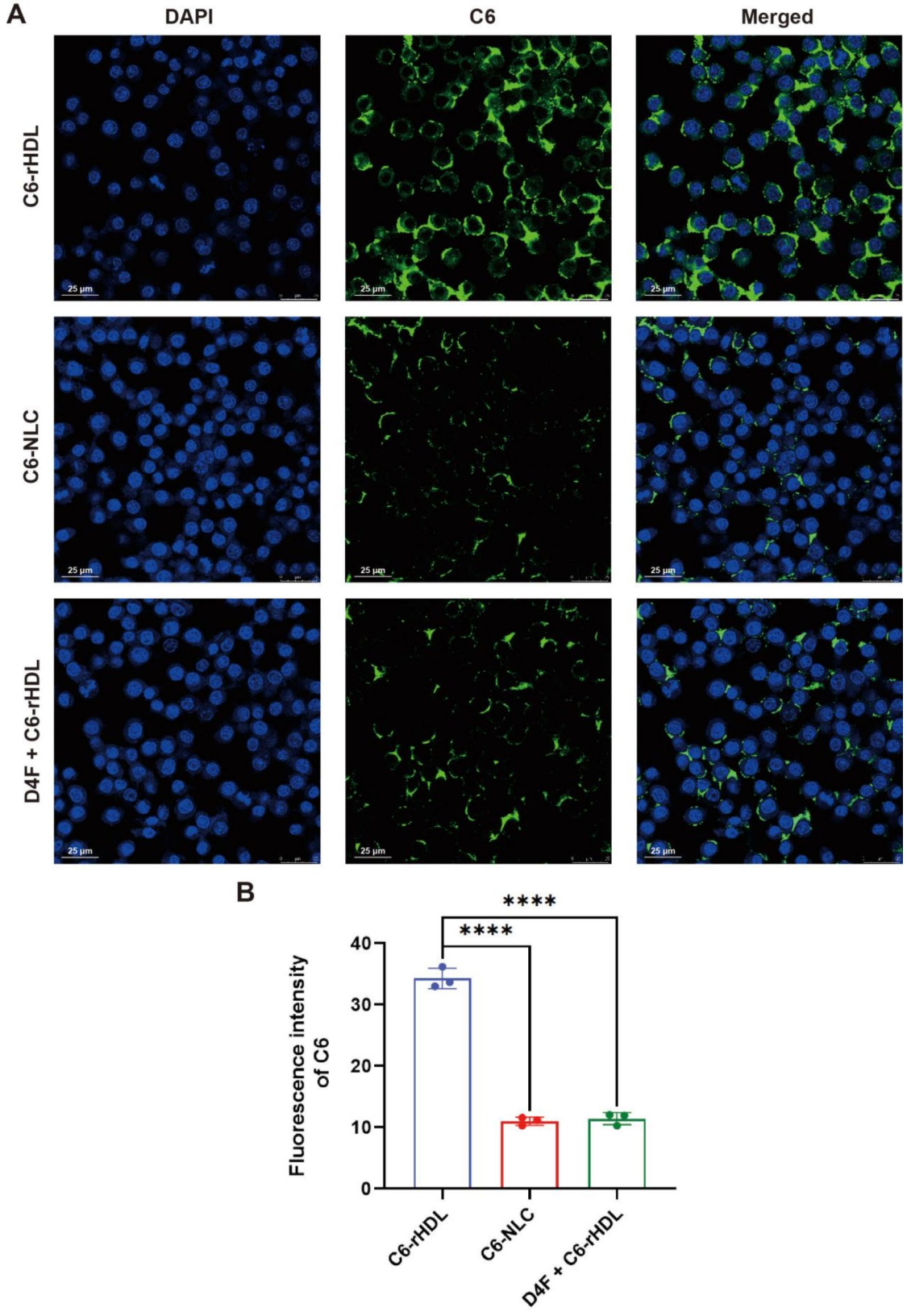

Fig. 4 C6-rHDL uptake and the quantification of C6 fluorescence intensity in foam cells (scale bar: 25 μm). ****$p < 0.0001$

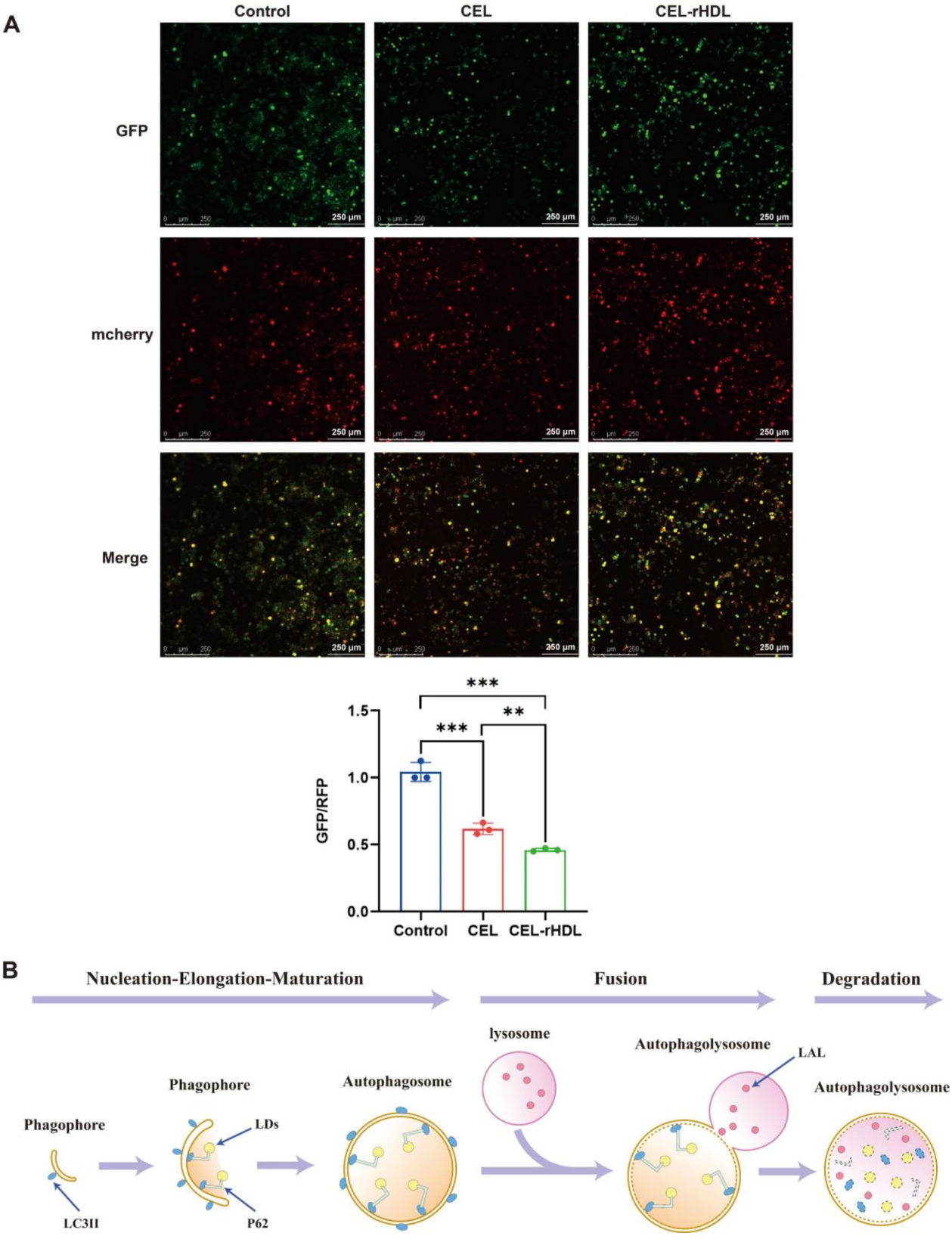

Fig. 5 (**A**) Fluorescence microscope image of mCherry-GFP-LC3 adenovirus transfection (scale bar: 250 μm). (**B**) The process of lipophagy. $^{**}p < 0.01$ and $^{***}p < 0.001$

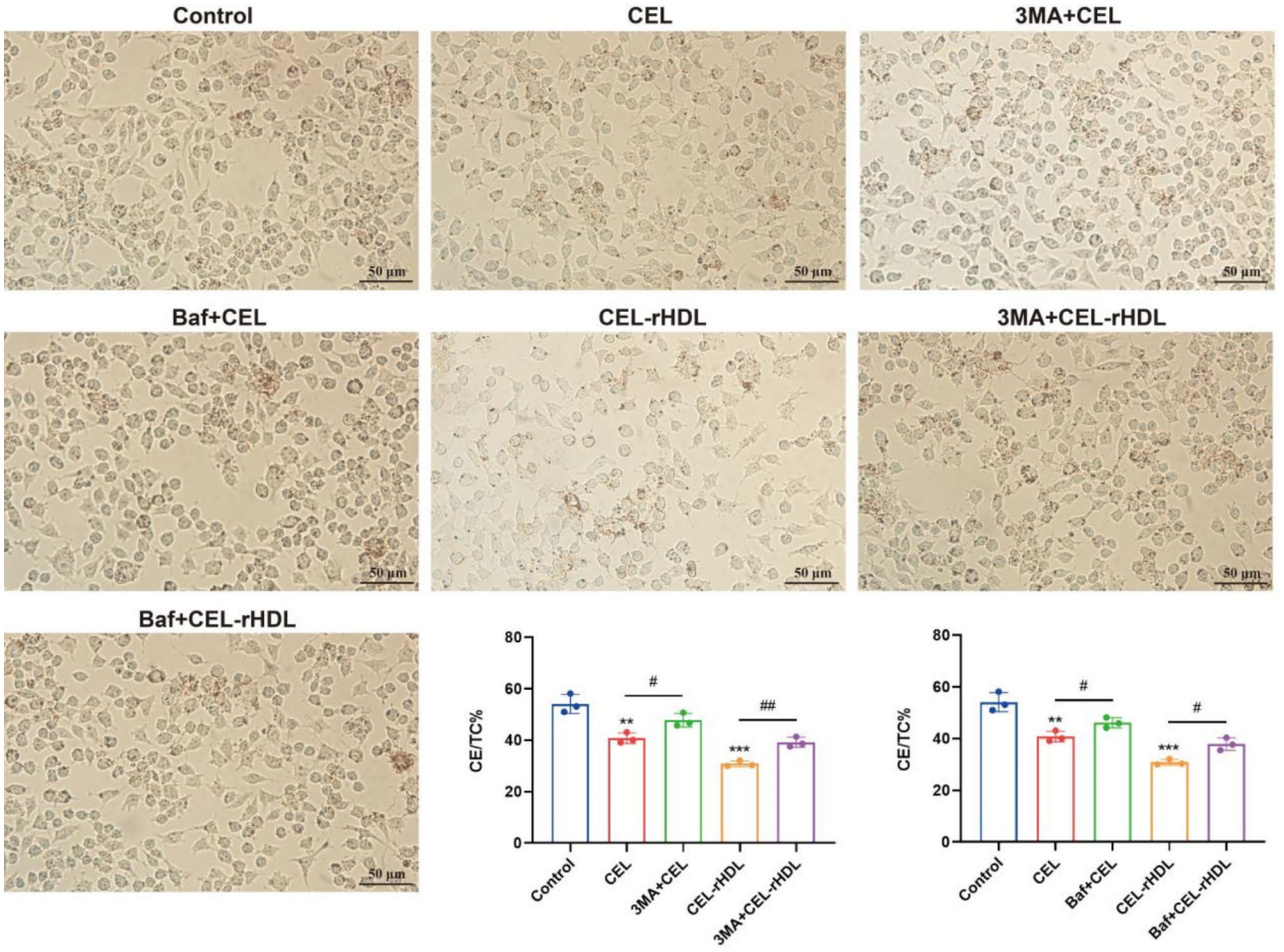

Fig. 6 Autophagy inhibitors inhibited the role of CEL or CEL-rHDL in foam cells. Oil Red O staining and CE quantification after treatment of 3-MA or Baf (scale bar: 50 μm). $^{**}p < 0.01$, $^{***}p < 0.001$ vs. Control; $\#p < 0.05$, $\#\#p < 0.01$, $\#\#\#p < 0.001$

indicated a direct relation between the cell cycle and lipid homeostasis. Lipids stored in LDs are mobilized when quiescent G0 phase cells resume cell division [51]. Besides, cyclin D1 serving as a key mediator of cell cycle progression was both necessary and sufficient to promote LDs accumulation in response to mitogens. Interestingly, cyclin D1 seemed to facilitate LDs accumulation by retarding lipolysis via a mechanism involving lessened lipophagy [52]. Additionally, the Kyoto Encyclopedia of Genes and Genomes (KEGG) enrichment analysis confirmed 20 pathways that were remarkably related to DEGs, containing cell cycle, mTOR signaling pathway, phagosome, lysosome, fluid shear stress and atherosclerosis (Fig. 8E). Phagosome and lysosome are two momentous organelles involved in the process of lipophagy. The phagosome encapsulated LDs stored in foam cells and then fused with lysosomes to form autolysosomes, in which LDs were degraded into FC by LAL. Serving as a classical signal node modulating lipophagy, mTOR has been shown to promote the formation of lipid-laden foam cells through inhibiting the lipophagic process, thereby accelerating the progression of atherosclerotic lesions [53]. As a vital upstream molecule of mTOR, AMPK mediates a variety of physiological processes, such as lipid and glucose metabolism as well as the normalization of energy imbalances, exhibiting therapeutic importance for treating CVD, obesity and type 2 diabetes [54–56]. Moreover, AMPK is also known to facilitate lipophagy by negatively regulating mTOR signaling pathway [57]. Therefore, it can be speculated that CEL-rHDL may induce lipophagy in foam cells to promote lipid degradation via mediating AMPK-mTOR signaling pathway.

qPCR analysis

To confirm the pathway identified by RNA-seq, the mRNA levels of CaMKKβ, AMPK, mTOR, LC3B and P62 were determined through qPCR. Ca^{2+}/CaMKKβ/AMPK/mTOR signaling pathway is a representative intracellular signaling pathway, which is involved in modulating multiple vital functions, including lipophagy, cell proliferation and apoptosis [58–60]. Ca^{2+} is a crucial intracellular messenger responsible for initiating a series of

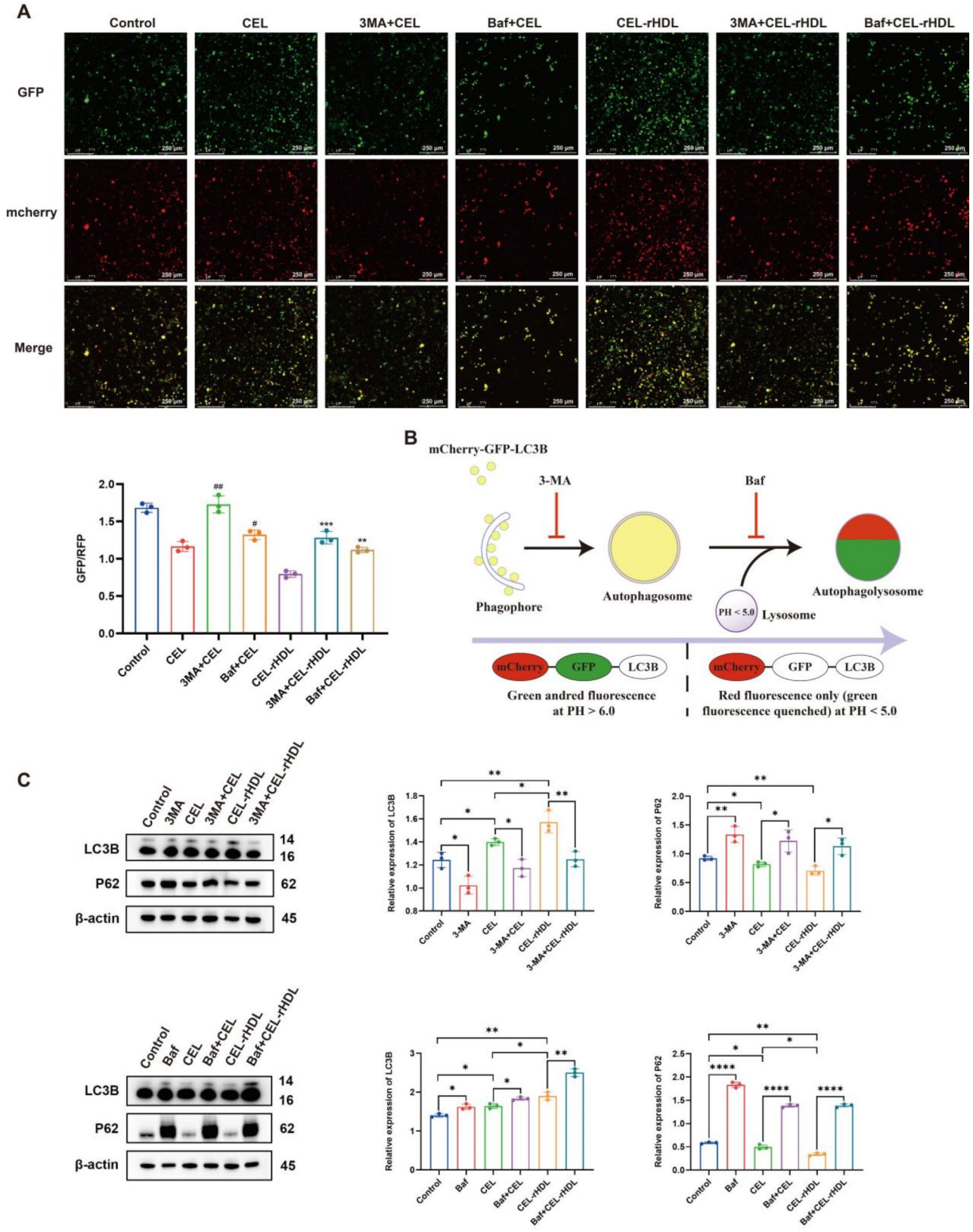

Fig. 7 Autophagy inhibitors inhibited the role of CEL or CEL-rHDL in foam cells. (**A**) Fluorescence microscopy images of mCherry-GFP-LC3 adenovirus transfection treated with CEL, 3MA + CEL, Baf + CEL, CEL-rHDL, 3MA + CEL-rHDL and Baf + CEL-rHDL (scale bar: 250 μm). (**B**) Schematic presentation of autophagy flux affected by 3MA (1.5 mM) and Baf (50 nM). (**C**) The changes of LC3B and P62 in foam cells treated with CEL or CEL-rHDL with or without 3MA or Baf. #$p < 0.05$, ##$p < 0.01$, ###$p < 0.001$ vs. CEL; *$p < 0.05$, **$p < 0.01$, ***$p < 0.001$ vs. CEL-rHDL

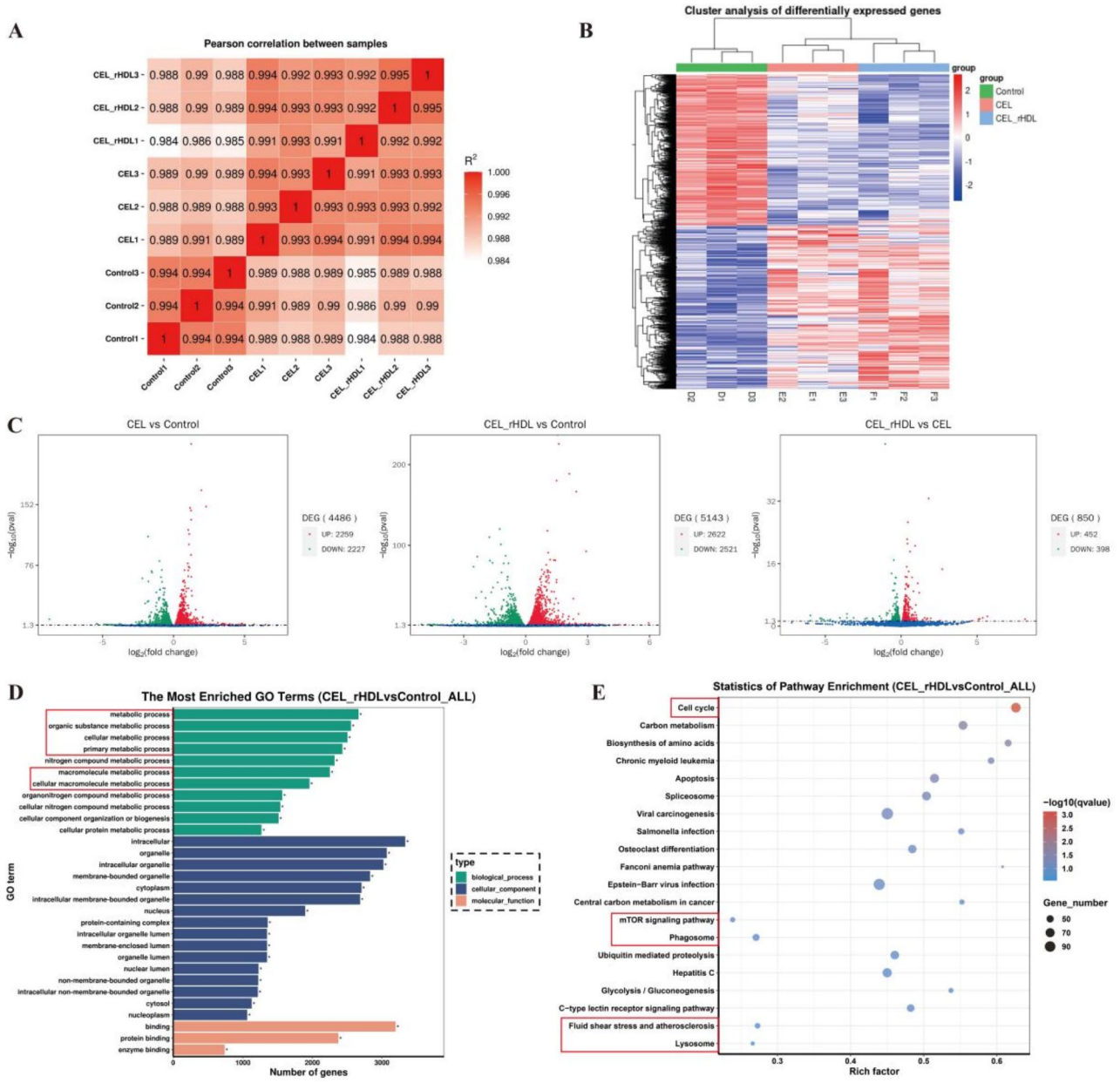

Fig. 8 RNA-seq analysis. (**A**) Correlation analysis of control, CEL and CEL-rHDL groups. (**B**) Clustering analysis of DEGs among control, CEL and CEL-rHDL groups. (**C**) The DEGs consequence. (**D**) The GO enrichment analysis. (**E**) The KEGG analysis

activities related to cellular metabolism and its homeostasis is essential for adipogenesis and lipid deposition [61, 62]. As one of the direct upstream kinases for AMPK, CaMKKβ phosphorylates and activates AMPK in response to elevated intracellular Ca^{2+} levels, as well as CaMKKβ could combine with AMPK to form a specific signaling complex [63, 64]. AMPK serves as a central modulator of a variety of metabolic pathways and may possess vital therapeutic significance in the treatment of CVD, diabetes and obesity [54]. It is also known to inhibit the downstream molecules such as mTOR, which is implicated in regulating lipid metabolism, autophagy and cellular proliferation [65]. In this study, the data suggested that levels of CaMKKβ, AMPK and LC3B were strongly upregulated in foam cells treated with CEL-rHDL compared to the other groups, while mTOR and P62 were significantly decreased, demonstrating that CEL-rHDL may induce foam cells lipophagy to reverse atherosclerosis by activating Ca^{2+}/CaMKKβ/AMPK/mTOR signaling pathway (Fig. 9).

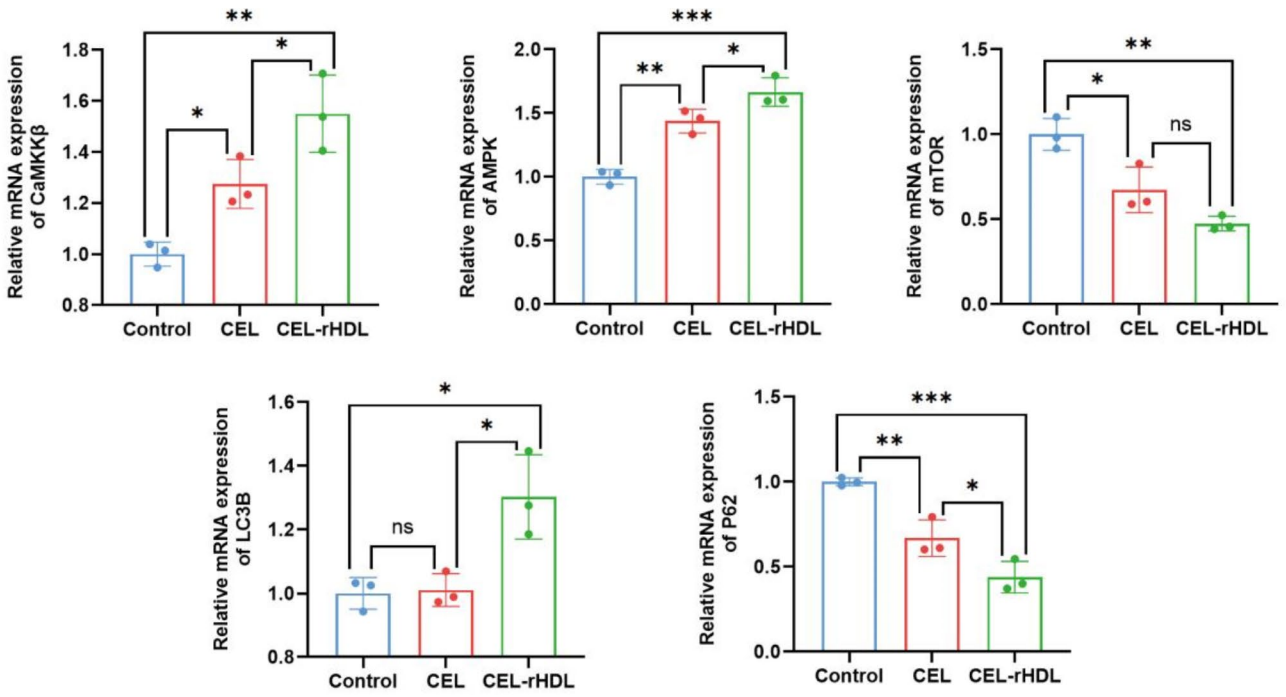

Fig. 9 Effects of CEL-rHDL on Ca^{2+}/CaMKKβ/AMPK/mTOR signaling pathway related mRNA expression. *$p < 0.05$, **$p < 0.01$ and ***$p < 0.001$

CEL-rHDL targets endoplasmic/sarcoplasmic reticulum (ER/SR) Ca^{2+} ATPase (SERCA) for Ca^{2+} mobilization to induce lipophagy

Recent studies have shown that CEL inhibited SERCA and stimulated Ca^{2+}-mediated autophagy to mitigate rheumatoid arthritis and suppress tumor growth [38, 66]. To investigate whether CEL-rHDL would generate analogous effects in foam cells, Fluo-4 AM was employed to detect the free Ca^{2+} levels in foam cells. As shown in Fig. 10A, foam cells loaded with Fluo 4-AM exhibited significantly elevation in fluorescence intensity upon the addition of 0.8 μM CEL and CEL-rHDL, and the fluorescence intensity of CEL-rHDL group surpassed CEL group. Moreover, pretreatment of foam cells with TG (1 μM), a SERCA-specific blocker, consumed SERCA-dependent Ca^{2+} storage and distinctly restrained CEL-rHDL-induced Ca^{2+} mobilization, confirming that CEL-rHDL induced the increase of cytoplasmic Ca^{2+} in SERCA-dependent manner.

To evaluate whether CEL-rHDL triggered an increase in cytoplasmic Ca^{2+} levels to yield lipophagy signaling, foam cells were treated with CEL and CEL-rHDL in the presence or absence of BAPTA/AM, a widely used intracellular Ca^{2+} chelator. In the presence of BAPTA/AM, the expression ratio of LC3-II/LC3-I was downregulated and P62 level was significantly upregulated (Fig. 10C-E), demonstrating that CEL-rHDL triggers lipophagy through a Ca^{2+}-dependent mechanism.

Ca^{2+}/CaMKKβ/AMPK/mTOR signaling pathway is involved in CEL-rHDL-induced lipophagy in foam cells

As an intracellular second messenger, free Ca^{2+} is regarded as a vital regulator of systemic lipid homeostasis, stimulating various proteases and kinases potentially involved in lipid metabolism, containing CaMKKβ [67]. CaMKKβ serves as a crucial upstream activator of AMPK, inducing AMPK activation via phosphorylating Thr172 in response to intracellular Ca^{2+} mobilization, and up-regulated AMPK negatively regulates mTOR to promote lipophagy [59]. The relevant proteins expression in foam cells treated with CEL and CEL-rHDL for indicated times was investigated. To verify the role of CaMKKβ in CEL-rHDL-induced lipophagy, foam cells were pretreated with STO-609 (CaMKKβ inhibitor) prior to exposure to CEL and CEL-rHDL. As shown in Fig. 11A, compared with the CEL and CEL-rHDL groups alone, pretreatment with STO-609 significantly declined p-AMPK and LC3-II/LC3-I levels, whereas markedly increased p-mTOR and P62 levels, suggesting a possible role of CaMKKβ in mediating CEL-rHDL-induced lipophagy. To investigate the participation of AMPK in CEL-rHDL-triggered lipophagy, CC (AMPK inhibitor) was employed to evaluate the role of CEL-rHDL on lipophagy. Compared with the CEL and CEL-rHDL groups alone, pretreatment with CC markedly reduced the LC3-II/LC3-I level, while evidently increased p-mTOR and P62 levels (Fig. 11B), confirming the participation of AMPK in CEL-rHDL-induced lipophagy. Above all, these results indicated that Ca^{2+}/CaMKKβ/AMPK/mTOR was

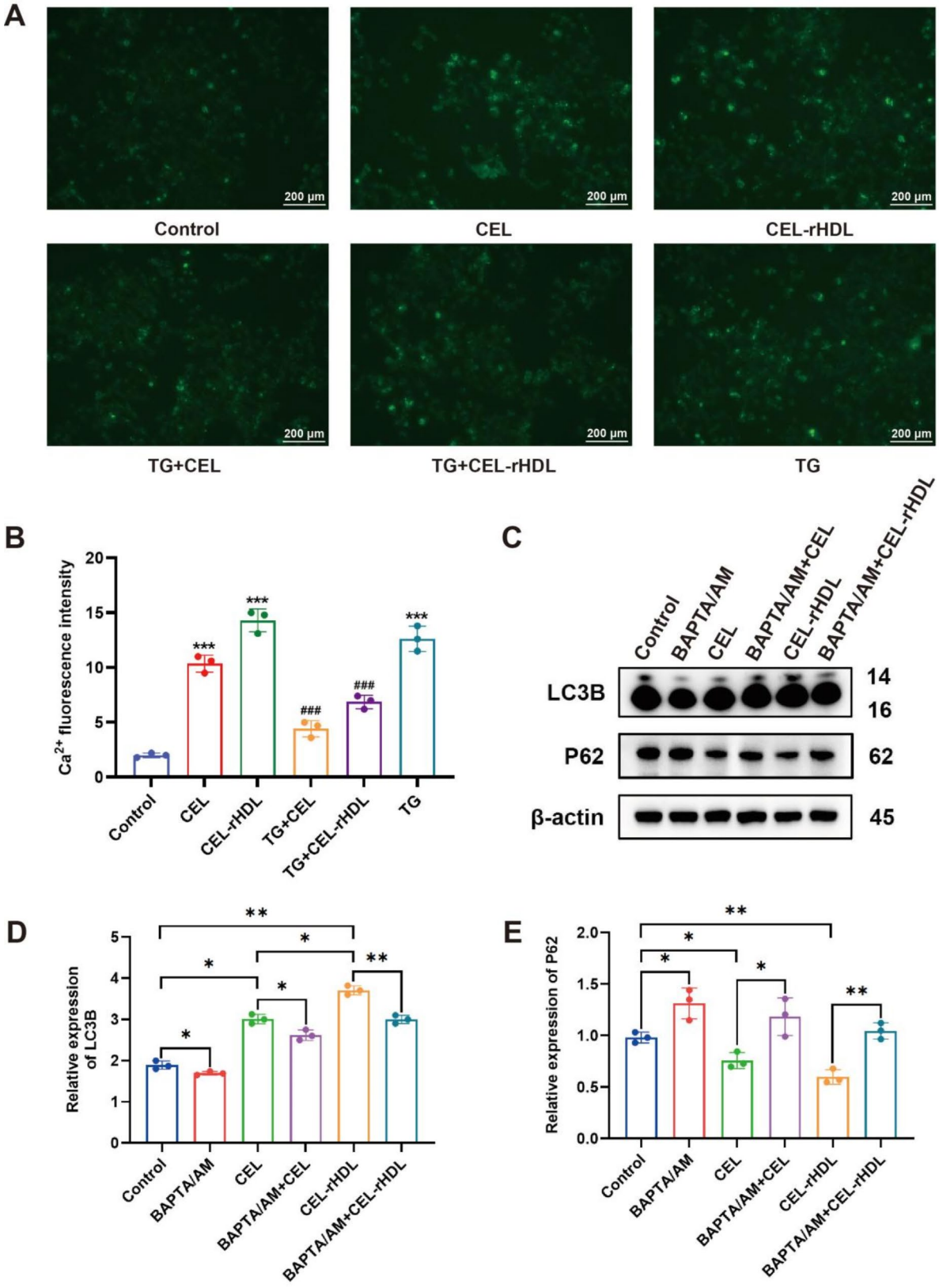

Fig. 10 (**A**) Ca^{2+} fluorescence images (scale bar: 200 μm). (**B**) The qualification of Ca^{2+} fluorescence intensity. (**C**-**E**) Western blot of LC3B and P62 in foam cells exposed to CEL or CEL-rHDL with or without 5 μM BAPTA/AM. *$p < 0.05$, **$p < 0.01$ and ***$p < 0.001$ vs. Control group; #$p < 0.05$, ##$p < 0.01$ and ###$p < 0.001$ vs. CEL or CEL-rHDL

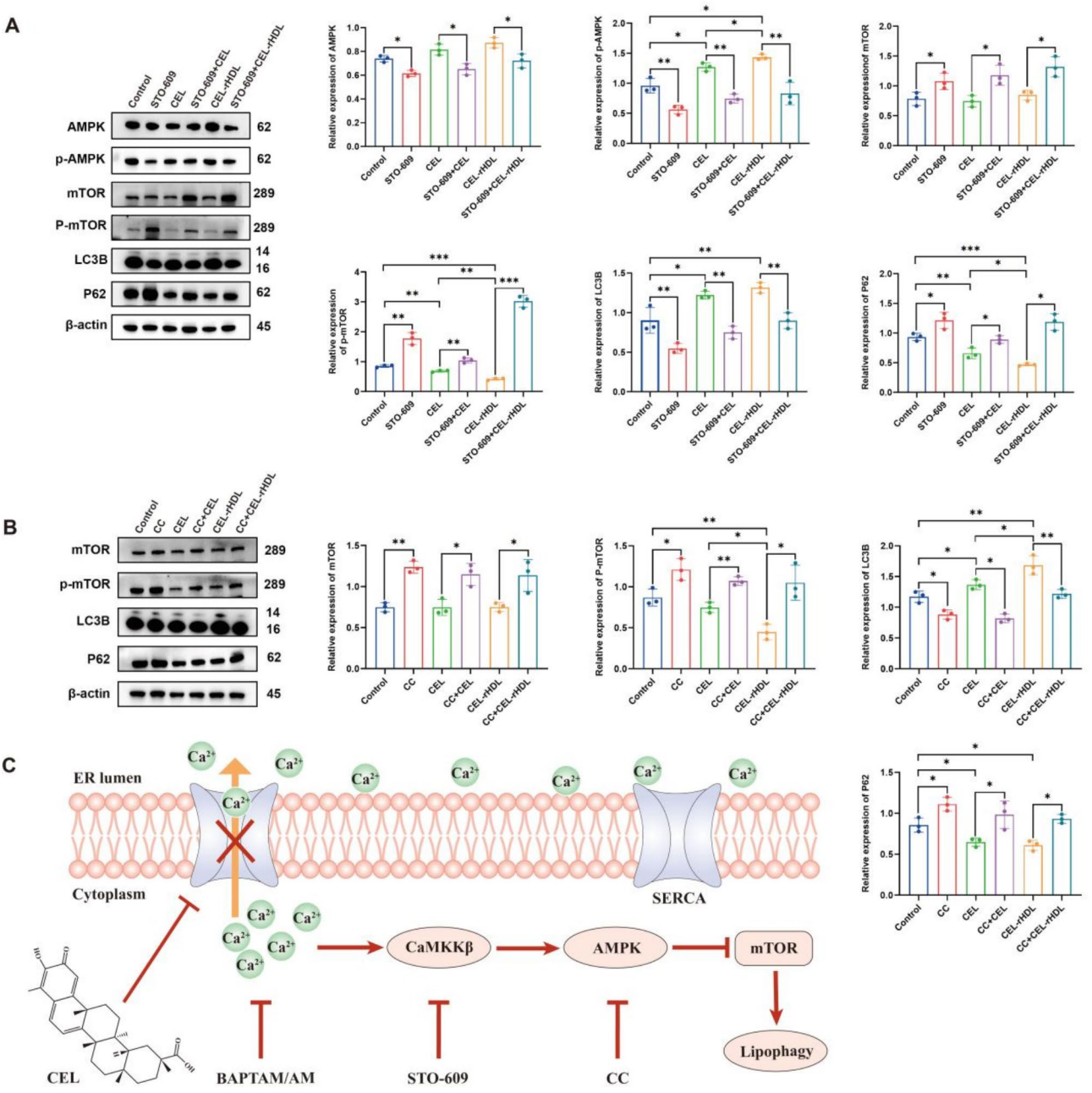

Fig. 11 Lipophagy induced by CEL-rHDL is related to the Ca^{2+}/CaMKKβ/AMPK/mTOR signaling pathway. (**A**) The changes of relevant proteins in foam cells treated with CEL or CEL-rHDL in the presence or absence of 25 μM STO-609. (**B**) The changes of relevant proteins in foam cells treated with CEL or CEL-rHDL in the presence or absence of 5 μM CC. (**C**) Schematic presentation of the signaling cascade to lipophagy. *$p < 0.05$, **$p < 0.01$ and ***$p < 0.001$

implicated in CEL-rHDL-induced lipophagy in foam cells.

rHDL promotes cholesterol efflux

RCT, an atheroprotective mechanism, drives FC moving from foam cells in arterial walls into the circulatory system for excretion in the feces [68, 69]. The first and perhaps most critical step of RCT is cholesterol efflux from foam cells, a process particularly associated with the regression of atherosclerotic plaques [70]. Next, we evaluated whether CEL, CEL-rHDL and rHDL could promote cholesterol efflux. NBD-cholesterol, a fluorescent sterol, was applied to incubate with foam cells and labeled cholesterol efflux to CEL, CEL-rHDL and rHDL was detected. As shown in Fig. 12, the effect of CEL-rHDL and rHDL stimulating cholesterol efflux from foam cells was considerable, and both were stronger than CEL.

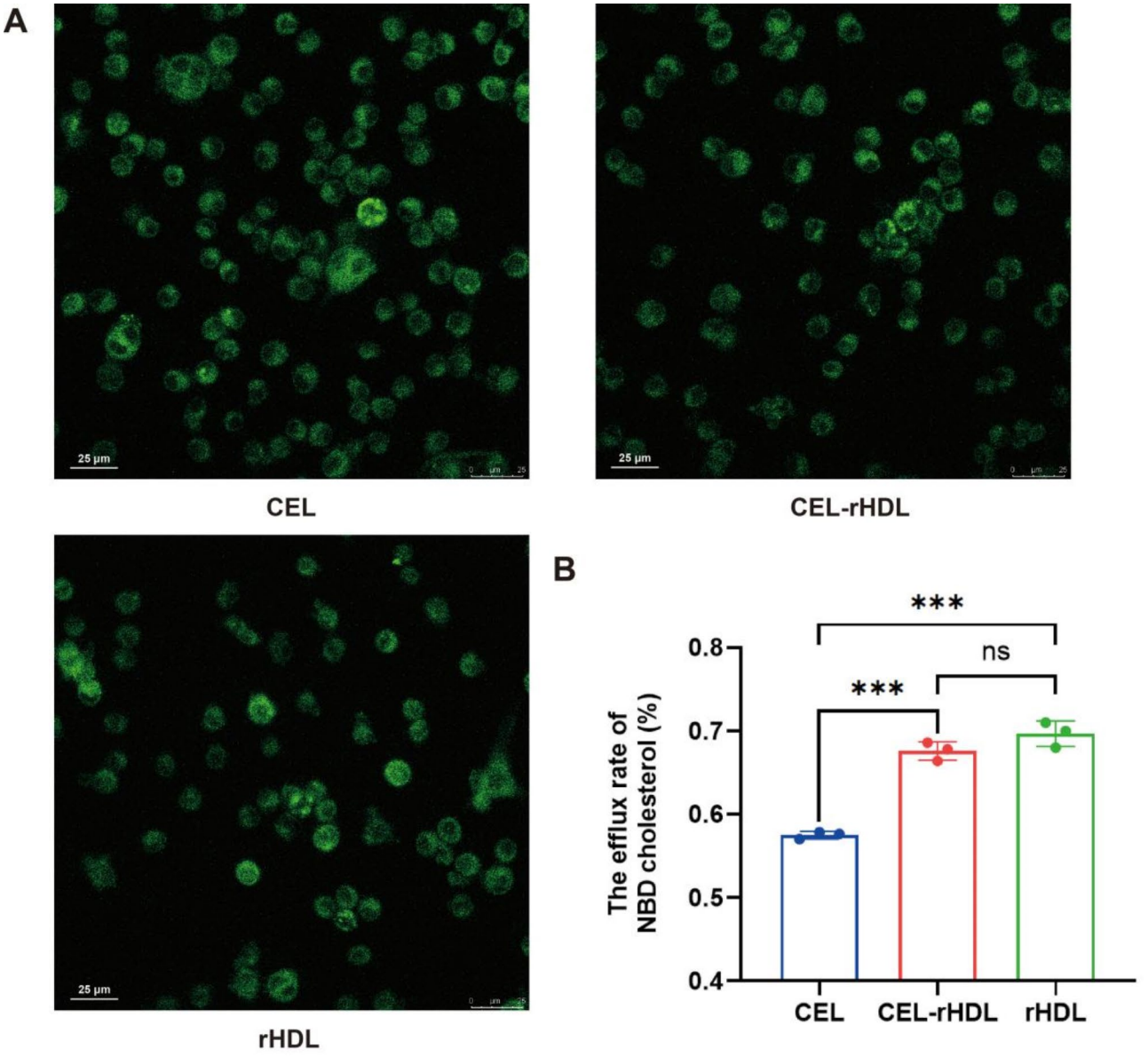

Fig. 12 (**A**) Representative fluorescent images of the NBD-cholesterol burden in foam cells obtained in corresponding group after incubation with CEL, CEL-rHDL and rHDL for 6 h (scale bar: 25 μm). (**B**) The efflux rate of NBD cholesterol efflux mediated by CEL, CEL-rHDL and rHDL

In vivo atherosclerotic lesions targeting and anti-atherosclerotic efficacy

To demonstrate the plaque targeting properties of CEL-rHDL, the Apo $E^{-/-}$ atherosclerotic mice were sacrificed to obtain aortic tree after 12 h injection and observe the degree of fluorescence aggregation. After 12 h injection of free DiR, there was nearly no fluorescence in the isolated aortic tree of Apo $E^{-/-}$ atherosclerotic mice. The fluorescence intensity in aortic tree after injection of CEL-rHDL/DiR exhibited significantly stronger than that in CEL-NLC/DiR group, indicating that CEL-rHDL owned the ability to actively target the atherosclerotic lesions region attributed to specific binding of D4F on the surface of CEL-rHDL with SR-BI, coinciding with the in vitro C6-rHDL uptake in foam cells (Fig. 13A). The major blood lipids and atherosclerotic plaques at various sites were measured to assess anti-atherosclerotic effects after 4 weeks of treatment with CEL and CEL-rHDL. Compared with normally fed Apo $E^{-/-}$ mice, the high-fat diet resulted in sharply higher levels of blood lipids (containing TC, TG and LDL-C) and the areas of atherosclerotic plaque at different sites, implying the successful construction of the atherosclerotic mouse model. After treatment with CEL and CEL-rHDL in atherosclerotic mice, the contents of TC, LDL-C and TG declined whereas the content of HDL-C elevated, showing the anti-atherosclerotic roles of these drugs, in which CEL-rHDL performed better (Fig. 13B). Furthermore, full-length aorta and

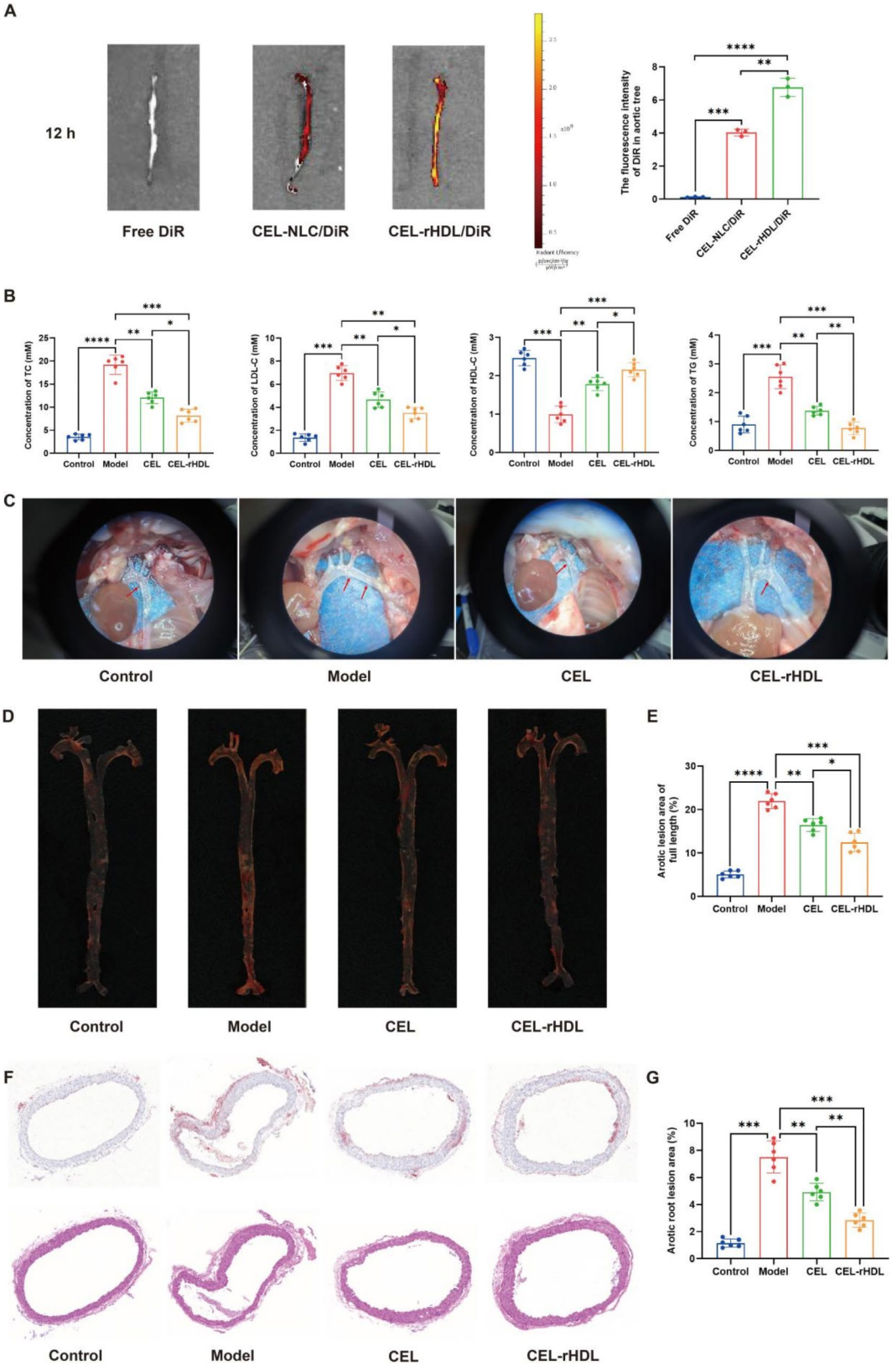

Fig. 13 (See legend on next page.)

(See figure on previous page.)

Fig. 13 In vivo atherosclertic lesions targeting and the suppressive effect of CEL-rHDL on atherosclerotic lesions formation. (**A**) In vivo image of aortic tree and quantitative analysis of the fluorescent intensity of DiR in aortic tree from Apo $E^{-/-}$ atherosclerotic mice administrated with free DiR, CEL-NLC/DiR and CEL-rHDL/DiR after 12 h injection ($n=3$). (**B**) The changes of major blood lipids concentrations in Apo $E^{-/-}$ mice ($n=6$). (**C**) The atherosclerotic plaques in aortic arches (red arrows). (**D**-**E**) Oil Red O staining and quantitative analysis of atherosclerotic lesions in full length aorta ($n=6$). (**F**) Oil Red O staining (upper panels) or H&E (bottom panels) of aortic root slices. (**G**) The quantitative test of Oil Red O staining in aortic root ($n=6$). *$p<0.05$, **$p<0.01$, ***$p<0.001$ and ****$p<0.0001$

aortic roots were stained with Oil Red O to assess plaque areas. Clearly, compared with the normal Apo $E^{-/-}$ mice, the atherosclerotic model mice developed severe atherosclerotic plaques in full-length aorta and aortic roots, while the atherosclerotic mice treated with CEL and especially CEL-rHDL, only minor atherosclerotic plaques occurred (Fig. 13C, D and F). The adjacent adipose tissue outside the lumen has been excluded during the calculation. The above data indicated the better suppressive effect of CEL-rHDL on atherosclerosis in high-fat fed mice.

Ca^{2+}/CaMKKβ/AMPK/mTOR signaling axis in vivo

To affirm the effect of CEL-rHDL on Ca^{2+}/CaMKKβ/AMPK/mTOR signaling axis in vivo, the expression of this pathway-related mRNA and protein was detected by qPCR and western blot. Compared with control or CEL-treated mice, CaMKKβ, AMPK and LC3B mRNA levels were upregulated significantly, while mTOR and P62 mRNA levels were downregulated after the addition of CEL-rHDL (Fig. 14A-E). Moreover, p-CaMKKβ, p-AMPK and LC3-II/LC3-I levels were elevated, p-mTOR and P62 were decreased after the treatment of CEL-rHDL, along with the total CaMKKβ, AMPK and mTOR levels unchanged (Fig. 14F-K).

In vivo safety evaluation

The toxicity of CEL and CEL-rHDL on the major organs of mice was assessed by H&E staining and blood biochemical parameters. Despite CEL exhibits promising anti-atherosclerotic activity, the clinical application of CEL is greatly limited due to its severe side effects. Hepatotoxicity and nephrotoxicity are the main serious side effects of CEL [71, 72]. As shown in Fig. 15A, no significant pathological changes were observed in the myocardial tissue, lung tissue and spleen tissue of mice in each group. However, the livers and kidneys of mice treated with free CEL were in poor condition, showing watery degeneration, inflammatory cell infiltration and individual focal necrosis of hepatocytes, and renal interstitial edema, inflammatory cell infiltration and renal tubule degeneration and atrophy. Moreover, compared with the control group, the CEL-rHDL group displayed only mild hepatocyte edema without serious side effects, and its severity was lower than that observed in the free CEL group. Furthermore, ALT, AST and BUN levels were distinctly elevated in free CEL group compared with the control group, whereas the CEL-rHDL group had no significant difference compared with the control group (Fig. 15B). Therefore, the safety evaluation demonstrated that CEL-rHDL could decrease the systemic toxicity of CEL and possess relatively biocompatibility.

Discussion

Atherosclerosis, characterized by abnormal lipid deposition within the subendothelial regions of arterial walls, underlies various cardiovascular and cerebrovascular diseases, which is a leading cause of death worldwide [73, 74]. Ox-LDL is identified as a major contributor to atherosclerosis, excessive uptake of which can trigger lipid accumulation and accelerate the formation of foam cells, which are a major component of atherosclerotic lesions and act a vital function in the development of atherosclerosis [24]. Recently, CEL has emerged as a promising hypolipidemic agent for the treatment of cardiovascular disease. Growing evidence indicated that CEL exhibited anti-atherosclerotic roles via modulating lipid metabolism, improving vascular function and decreasing oxidative stress [75, 76]. Despite CEL possesses good regulatory effects on lipid metabolic disorders, the pharmaceutical potential of CEL is severely influenced by its strong hydrophobicity and off-target toxicity [77]. Here, CEL was loaded into rHDL to entable targeted delivery to foam cells, while CEL-rHDL was further assessed for the therapeutic potential in a high-fat diet-induced mouse model of atherosclerosis, and how lipophagic initiation acted on lipid metabolism and RCT process were elucidated in vitro, even the detailed mechanism in molecular levels.

In the present study, D4F, an Apo AI mimetic peptide, contained 18 amino acids and owned class A amphipathic helix with a polar and a non-polar face, enabling it to bind lipids for the formation of HDL-like particles [78]. We have successfully constructed rHDL to load CEL with a similar microstructure to natural HDL, which owned suitable particle size, high EE and comparable DL. In serum stability and blood compatibility assays, CEL-rHDL manifested satisfactory stability in terms of particle size and zeta potential in FBS, as well as favourable biocompatibility. The assembled nanoparticles with negative potential could evade the attack of plasma components until finally arriving at the specific atherosclerotic lesions, due to which make them more stable in plasma. Meanwhile, CEL-rHDL exhibited markedly higher

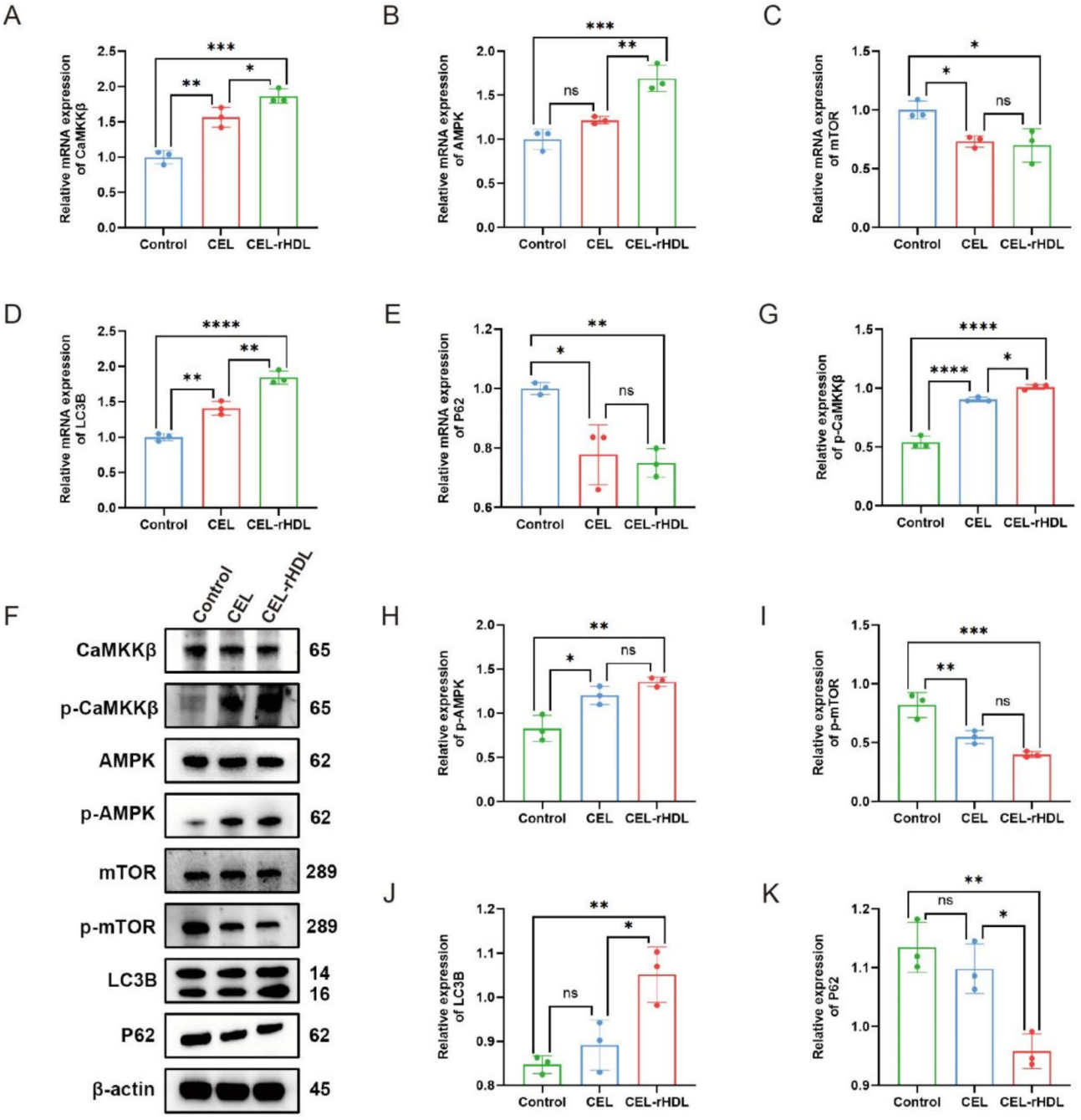

Fig. 14 Effects of CEL-rHDL on Ca^{2+}/CaMKKβ/AMPK/mTOR signaling pathway related mRNA and proteins in vivo (The samples were derived from thoracic aorta tissue of Apo $E^{-/-}$ atherosclerotic mice). (**A**-**E**) qPCR results of CaMKKβ, AMPK, mTOR, LC3B and P62 in each group. (**F**-**K**) The western blot results. *$p < 0.05$, **$p < 0.01$, ***$p < 0.001$ and ****$p < 0.0001$

cellular uptake efficiency in foam cells and showed favorable atherosclerotic plaques-targeting in vivo. SR-BI as an integral membrane protein is overexpressed in foam cells of atherosclerotic lesions that can be specifically recognized by D4F [14]. Based on high affinity between D4F and SR-BI, CEL-rHDL effectively enhanced the accumulation of CEL in foam cells. Besides, in drug release assay, the release rate of CEL from CEL-rHDL was significantly greater under acidic conditions compared to neutral conditions, which might be attributed to the structural and functional changes of D4F under an acidic environment, followed by the release of CEL. At last, cholesterol efflux assay revealed that rHDL could facilitate the cholesterol efflux from foam cells more effectively than CEL alone. The FC generated through lipophagy needs to be promptly moved from foam cells, a key step of RCT,

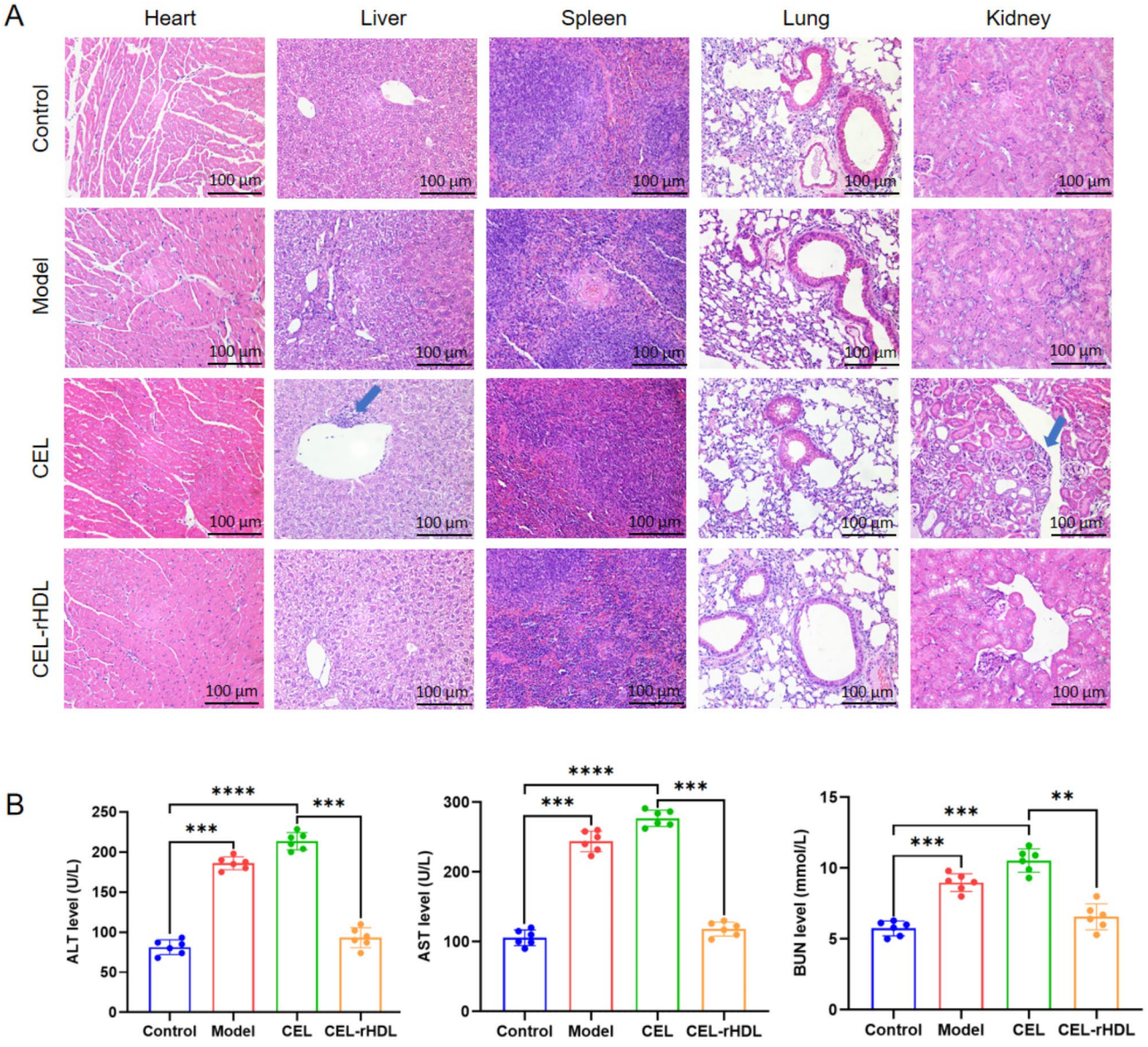

Fig. 15 (**A**) H&E staining of different organs in Apo $E^{-/-}$ mice treated with normal saline, free CEL and CEL-rHDL (scale bar: 100 μm). Blue arrows were used to indicate the lesions in sections stained with H&E. (**B**) ALT, AST and BUN levels in Apo $E^{-/-}$ mice treated with normal saline, free CEL and CEL-rHDL ($n = 6$). $^{**}p < 0.01$, $^{***}p < 0.001$ and $^{****}p < 0.0001$

which provides an effective way for alleviating the lipid burden of foam cells. In this process, the circulated rHDL served as drug targeting carriers, alternatively acted as FC receptors to exert RCT roles.

The accumulation of lipid-rich foam cells in arterial walls involves in the initiation of atherosclerotic lesions, the progression of plaque and the occurrence of lethal complications in advanced stage [79]. LDs, as the main site of cholesterol storage in foam cells, are a potential therapeutic target for atherosclerosis. Research have highlighted the essential roles of lipophagy in lipid metabolism, offering a therapeutic regimen on atherosclerotic pathogenesis [44, 80, 81]. In our study, compared to the CEL group, CEL-rHDL markedly reduced P62 expression and increased the transition of LC3 from type I to type II. The effect was further evaluated by transfecting mCherry-GFP-LC3 adenovirus into foam cells to observe autophagy flux, from which CEL-rHDL significantly decreased the ratio of GFP to RFP, showing an elevation in lipophagy. Conclusively, CEL-rHDL may attenuate lipid deposition in foam cells via promoting lipophagy, consistent with previously reported studies on CEL [75, 82]. To further confirm the function of CEL-rHDL in lipophagy, 3-MA and Baf (two autophagy inhibitors) were applied to block lipophagy, lipid deposition in foam cells treated with CEL-rHDL was significantly

higher than that without the blockage of lipophagy. Additionally, the ratio of GFP to RFP increased markedly in CEL-rHDL treated foam cells after lipophagy blockage, demonstrating an alleviation of intracellular lipid accumulation is dependent on lipophagy.

To elucidate the exact mechanism on how CEL-rHDL induced lipophagy, RNA-seq and qPCR were performed on macrophage-derived foam cells. RNA-seq data demonstrated that CEL-rHDL was implicated in several metabolic processes in foam cells, including cell cycle, intracellular phagosome formation and lysosome biogenesis, through mediating the mTOR signaling pathway. qPCR showed that CEL-rHDL significantly heightened the mRNA levels of CaMKKβ, AMPK and LC3B, while lessening the mRNA level of mTOR and P62. Simultaneously, western blot analysis further confirmed proteins expression related to lipophagy pathway. Our results revealed that CEL-rHDL upregulated AMPK by increasing CaMKKβ phosphorylation, subsequently restraining the expression of downstream protein mTOR. As a classical regulator of autophagy, mTOR is modulated by various upstream signal transduction factors, including AMPK. AMPK, a pivotal metabolic sensor, is widely recognized as regulators and guardians of lipid homeostasis. The upregulation of AMPK activity contributes to the mitigate metabolic diseases (containing atherosclerosis, obesity and NAFLD) associated with massive lipid generation [59, 83–85]. CaMKKβ, a calcium-sensitive kinase, phosphorylates and activates AMPK in response to elevated intracellular Ca^{2+} levels, as well as CaMKKβ could combine with AMPK to form a specific signaling complex [63, 64]. As a pivotal secondary messenger with comprehensive roles, Ca^{2+} initiates a range of fundamental activities on systemic lipid homeostasis, based on which is essential for lipid-related metabolic diseases [61, 86]. Abnormal Ca^{2+} deposition surrounding the cytoplasmic LDs in hypertrophic adipocytes of obese mice has been proved, and adipocytes derived from obese elderly people also showed an increase in cytoplasmic Ca^{2+} levels, probably suggesting enhanced Ca^{2+} levels in the case of intracellular lipid accumulation [87, 88]. It is worth noting that the elevation in cytoplasmic Ca^{2+} contributes to transducing a lipolytic signal to stimulate the occurrence of lipophagy [88]. The ER is the major site of Ca^{2+} storage and exerts a vital role in maintaining intracellular Ca^{2+} homeostasis. SERCA, a membrane Ca^{2+} transporter, pumps cytoplasmic Ca^{2+} into the lumen of SR/ER to maintain the stable levels of cytoplasmic Ca^{2+} concentrations, and the suppression of SERCA could induce autophagy in cancer cells [38, 89, 90]. Previous studies have demonstrated that CEL inhibits SERCA to promote the increase of cytoplasmic Ca^{2+} level [38, 66].

In this study, we found that the administration of either CEL-rHDL or TG alone induced a similar Ca^{2+} mobilization effect in foam cells. Whereas, pre-incubation of foam cells with TG to consume SERCA-dependent Ca^{2+} storage markedly refrained the CEL-rHDL-induced Ca^{2+} mobilization. Furthermore, chelating cytoplasmic Ca^{2+} by BAPTA/AM significantly abolished the elevation in LC3-II/LC3-I ratio and P62 degradation, suggesting that CEL-rHDL may promote lipophagy in a SERCA-mediated Ca^{2+} mobilization manner, which was also verified in the previous reports on CEL [38, 66]. As a direct upstream activator of AMPK, CaMKKβ could stimulate AMPK phosphorylation at Thr172 site in response to enhanced cytoplasmic Ca^{2+} levels [64]. Our study indicated that CEL-rHDL could upregulate CaMKKβ phosphorylation to enhance the expression of p-AMPK. Nevertheless, the above phenomenon was reversed by the CaMKKβ inhibiter STO-609, demonstrating that the lipid-lowering effect of CEL-rHDL in foam cells was mediated by CaMKKβ activation. Additionally, AMPK is well-established regulator of lipophagy, primarily through the downregulation of mTOR phosphorylation [91]. Our results suggested that the AMPK inhibitor CC abolished CEL-rHDL-mediated inhibition of mTOR phosphorylation. Collectively, it can be inferred that Ca^{2+}/CaMKKβ/AMPK/mTOR signaling pathway may be engaged in lipophagy induced by CEL-rHDL to decrease lipid accumulation in macrophage-derived foam cells.

Conclusion

In total, we successfully developed a CEL-loaded rHDL nanoparticle for targeted delivery of CEL to atherosclerotic lesions without obvious systemic toxicity. This mechanism might be explained that CEL-rHDL restrained lipid storage in foam cells through modulating Ca^{2+}/CaMKKβ/AMPK/mTOR signaling pathway to induce lipophagy. Besides, rHDL sequentially served as FC receptor for reversed transporting FC generated by lipophagy to the liver for timely metabolism. It provided a new insight into the atherosclerotic treatment to explore the potential of CEL-based hypolipidemic effect combined with rHDL carrier against early atherosclerosis. The green synthetic rHDL carrier is a mimic of endogenous HDL with biocompatible and biodegradable properties, which propose a precision therapeutic strategy on early atherosclerosis combined with chemodrugs and nanobiotechnology. However, for further clinical translation and industrial applications, on the basis of guaranteed efficiency, the synthetic processes should be simplified for easy-to-apply, and the preparation cost should be economically considered.

Acknowledgements

A special thanks for the long-term subsidy mechanism from the Ministry of Finance and the Ministry of Education of People's Republic of China for Beijing University of Chinese Medicine and China Academy of Chinese Medical Sciences.

Author contributions
Yang Li: writing-original draft, ideas, investigation; Xiaoxia Xue, Liuchunyang Yu: methodology; Jinxiu Qian, Xiaoyu Li: data curation; Meng Tian, Jue Yang, Rongjun Deng: Formal analysis; Cheng Lu, Yuanyan Liu: writing-reviewing and editing, project administration, conceptualization; Cheng Xiao: funding acquisition, conceptualization.

Funding
This work was supported by the Innovation Team and Talents Cultivation Program of National Administration of Traditional Chinese Medicine (No. ZYYCXTD-D-202005), the Youth Qihuang Scholar of National Administration of Traditional Chinese Medicine (2020), and the National Natural Science Foundation of China (Grant number: U22A20374).

Data availability
No datasets were generated or analysed during the current study.

Declarations

Competing interests
The authors declare no competing interests.

Author details
[1]School of Chinese Materia Medica, Beijing University of Chinese Medicine, Beijing, China
[2]Institute of Basic Research in Clinical Medicine, China Academy of Chinese Medical Sciences, Beijing, China
[3]Institute of Clinical Medicine, China-Japan Friendship Hospital, Beijing, China

Received: 22 December 2024 / Accepted: 13 March 2025
Published online: 22 March 2025

References

1. Wang K, Yu C, Liu Y, Zhang W, Sun Y, Chen Y. Enhanced antiatherosclerotic efficacy of Statin-Loaded reconstituted High-Density lipoprotein via ganglioside GM1 modification. ACS Biomater Sci Eng. 2018;4:952–62.
2. Robichaud S, Rasheed A, Pietrangelo A, Doyoung Kim A, Boucher DM, Emerton C, Vijithakumar V, Gharibeh L, Fairman G, Mak E, et al. Autophagy is differentially regulated in leukocyte and nonleukocyte foam cells during atherosclerosis. Circ Res. 2022;130:831–47.
3. Chen Y, Yu F, Zhang Y, Li M, Di M, Chen W, Liu X, Zhang Y, Zhang M. Traditional Chinese medication Tongxinluo attenuates lipidosis in Ox-LDL-Stimulated macrophages by enhancing Beclin-1-Induced autophagy. Front Pharmacol. 2021;12:673366.
4. Shao B, Han B, Zeng Y, Su D, Liu C. The roles of macrophage autophagy in atherosclerosis. Acta Pharmacol Sin. 2016;37:150–6.
5. Sukhorukov VN, Khotina VA, Chegodaev YS, Ivanova E, Sobenin IA, Orekhov AN. Lipid metabolism in macrophages: focus on atherosclerosis. Biomedicines. 2020;8:262.
6. Zuo J, Guo S, Qin X. Bisdemethoxycurcumin suppresses the progression of atherosclerosis and VSMC-derived foam cell formation by promoting lipophagy. Naunyn Schmiedebergs Arch Pharmacol. 2023;396:3659–70.
7. Tao J, Yang P, Xie L, Pu Y, Guo J, Jiao J, Sun L, Lu D. Gastrodin induces lysosomal biogenesis and autophagy to prevent the formation of foam cells via AMPK-FoxO1-TFEB signalling axis. J Cell Mol Med. 2021;25:5769–81.
8. Simonsen JB. Evaluation of reconstituted high-density lipoprotein (rHDL) as a drug delivery platform - a detailed survey of rHDL particles ranging from biophysical properties to clinical implications. Nanomedicine. 2016;12:2161–79.
9. Maugeais C, Annema W, Blum D, Mary J-L, Tietge UJF. rHDL administration increases reverse cholesterol transport in mice, but is not additive on top of Ezetimibe or Cholestyramine treatment. Atherosclerosis. 2013;229:94–101.
10. Zanotti I, Potì F, Cuchel M. HDL and reverse cholesterol transport in humans and animals: lessons from pre-clinical models and clinical studies. Biochim Biophys Acta Mol Cell Biol Lipids. 2022;1867:159065.
11. Mo Z-C, Ren K, Liu X, Tang Z-L, Yi G-H. A high-density lipoprotein-mediated drug delivery system. Adv Drug Deliv Rev. 2016;106:132–47.
12. Rong T, Wei B, Ao M, Zhao H, Li Y, Zhang Y, Qin Y, Zhou J, Zhou F, Chen Y. Enhanced Anti-Atherosclerotic efficacy of pH-Responsively releasable ganglioside GM3 delivered by reconstituted High-Density lipoprotein. Int J Mol Sci. 2021;22:13624.
13. Delk SC, Chattopadhyay A, Escola-Gil JC, Fogelman AM, Reddy ST. Apolipoprotein mimetics in cancer. Semin Cancer Biol. 2021;73:158–68.
14. Ma X, Song Q, Gao X. Reconstituted high-density lipoproteins: novel biomimetic nanocarriers for drug delivery. Acta Pharm Sin B. 2018;8:51–63.
15. Li Y, Luo X, Hua Z, Xue X, Wang X, Pang M, Wang T, Lyu A, Liu Y. Apolipoproteins as potential communicators play an essential role in the pathogenesis and treatment of early atherosclerosis. Int J Biol Sci. 2023;19:4493–510.
16. Park H-J, Kuai R, Jeon EJ, Seo Y, Jung Y, Moon JJ, Schwendeman A, Cho S-W. High-density lipoprotein-mimicking nanodiscs carrying peptide for enhanced therapeutic angiogenesis in diabetic hindlimb ischemia. Biomaterials. 2018;161:69–80.
17. Huang J-L, Jiang G, Song Q-X, Gu X, Hu M, Wang X-L, Song H-H, Chen L-P, Lin Y-Y, Jiang D, et al. Lipoprotein-biomimetic nanostructure enables efficient targeting delivery of SiRNA to Ras-activated glioblastoma cells via macropinocytosis. Nat Commun. 2017;8:15144.
18. Kuai R, Li D, Chen YE, Moon JJ, Schwendeman A. High-Density lipoproteins: Nature's multifunctional nanoparticles. ACS Nano. 2016;10:3015–41.
19. Zhang W-L, Xiao Y, Liu J-P, Wu Z-M, Gu X, Xu Y-M, Lu H. Structure and remodeling behavior of drug-loaded high density lipoproteins and their atherosclerotic plaque targeting mechanism in foam cell model. Int J Pharm. 2011;419:314–21.
20. Vucic E, Rosenson RS. Recombinant high-density lipoprotein formulations. Curr Atheroscler Rep. 2011;13:81–7.
21. Tardy C, Goffinet M, Boubekeur N, Ackermann R, Sy G, Bluteau A, Cholez G, Keyserling C, Lalwani N, Paolini JF, et al. CER-001, a HDL-mimetic, stimulates the reverse lipid transport and atherosclerosis regression in high cholesterol diet-fed LDL-receptor deficient mice. Atherosclerosis. 2014;232:110–8.
22. Li Z, Zhang J, Duan X, Zhao G, Zhang M, Celastrol. A promising agent fighting against cardiovascular diseases. Antioxid (Basel). 2022;11:1597.
23. Tan J-L, Yi J, Cao X-Y, Wang F-Y, Xie S-L, Zhou L-L, Qin L, Dai A-G. Celastrol: The new dawn in the treatment of vascular remodeling diseases. Biomed Pharmacother. 2023; 158:114177.
24. Gu J, Shi Y-N, Zhu N, Li H-F, Zhang C-J, Qin L. Celastrol functions as an emerging manager of lipid metabolism: mechanism and therapeutic potential. Biomed Pharmacother. 2023;164:114981.
25. Zhang Y, Geng C, Liu X, Li M, Gao M, Liu X, Fang F, Chang Y. Celastrol ameliorates liver metabolic damage caused by a high-fat diet through Sirt1. Mol Metab. 2017;6:138–47.
26. Choi SK, Park S, Jang S, Cho HH, Lee S, You S, Kim S-H, Moon H-S. Cascade regulation of PPARγ(2) and C/EBPα signaling pathways by Celastrol impairs adipocyte differentiation and stimulates lipolysis in 3T3-L1 adipocytes. Metabolism. 2016;65:646–54.
27. Igarashi M, Osuga J, Uozaki H, Sekiya M, Nagashima S, Takahashi M, Takase S, Takanashi M, Li Y, Ohta K, et al. The critical role of neutral cholesterol ester hydrolase 1 in cholesterol removal from human macrophages. Circ Res. 2010;107:1387–95.
28. Liu K, Czaja MJ. Regulation of lipid stores and metabolism by lipophagy. Cell Death Differ. 2013;20:3–11.
29. Ouimet M, Franklin V, Mak E, Liao X, Tabas I, Marcel YL. Autophagy regulates cholesterol efflux from macrophage foam cells via lysosomal acid lipase. Cell Metab. 2011;13:655–67.
30. Kumar S, Nanduri R, Bhagyaraj E, Kalra R, Ahuja N, Chacko AP, Tiwari D, Sethi K, Saini A, Chandra V, et al. Vitamin D3-VDR-PTPN6 axis mediated autophagy contributes to the Inhibition of macrophage foam cell formation. Autophagy. 2021;17:2273–89.
31. Ma Y, Huang Z, Zhou Z, He X, Wang Y, Meng C, Huang G, Fang N. A novel antioxidant Mito-Tempol inhibits ox-LDL-induced foam cell formation through restoration of autophagy flux. Free Radic Biol Med. 2018;129:463–72.
32. Zahid MDK, Rogowski M, Ponce C, Choudhury M, Moustaid-Moussa N, Rahman SM. CCAAT/enhancer-binding protein beta (C/EBPβ) knockdown reduces inflammation, ER stress, and apoptosis, and promotes autophagy in oxLDL-treated RAW264.7 macrophage cells. Mol Cell Biochem. 2020;463:211–23.
33. Liu L, He H, Zhang M, Zhang S, Zhang W, Liu J. Hyaluronic acid-decorated reconstituted high density lipoprotein targeting atherosclerotic lesions. Biomaterials. 2014;35:8002–14.
34. Wei B, Li Y, Ao M, Shao W, Wang K, Rong T, Zhou Y, Chen Y. Ganglioside GM3-Functionalized reconstituted High-Density lipoprotein (GM3-rHDL) as a novel nanocarrier enhances antiatherosclerotic efficacy of Statins in apoE-/-C57BL/6 mice. Pharmaceutics. 2022;14:2534.

35. Jiang C, Wang X, Teng B, Wang Z, Li F, Zhao Y, Guo Y, Zeng Q. Peptide-Targeted High-Density lipoprotein nanoparticles for combinatorial treatment against metastatic breast cancer. ACS Appl Mater Interfaces. 2021;13:35248–65.
36. Wang W, Chen K, Su Y, Zhang J, Li M, Zhou J. Lysosome-Independent intracellular drug/gene codelivery by Lipoprotein-Derived nanovector for synergistic Apoptosis-Inducing Cancer-Targeted therapy. Biomacromolecules. 2018;19:438–48.
37. Gu X, Zhang W, Liu J, Shaw JP, Shen Y, Xu Y, Lu H, Wu Z. Preparation and characterization of a lovastatin-loaded protein-free nanostructured lipid carrier resembling high-density lipoprotein and evaluation of its targeting to foam cells. AAPS PharmSciTech. 2011;12:1200–8.
38. Xu S-W, Law BYK, Qu SLQ, Hamdoun S, Chen J, Zhang W, Guo J-R, Wu A-G, Mok SWF, Zhang DW, et al. SERCA and P-glycoprotein Inhibition and ATP depletion are necessary for celastrol-induced autophagic cell death and collateral sensitivity in multidrug-resistant tumor cells. Pharmacol Res. 2020;153:104660.
39. Cai C, Zhu H, Ning X, Li L, Yang B, Chen S, Wang L, Lu X, Gu D. LncRNA ENST00000602558.1 regulates ABCG1 expression and cholesterol efflux from vascular smooth muscle cells through a p65-dependent pathway. Atherosclerosis. 2019;285:31–9.
40. Jiang C, Qi Z, Tang Y, Jia H, Li Z, Zhang W, Liu J. Rational design of Lovastatin-Loaded spherical reconstituted high density lipoprotein for efficient and safe Anti-Atherosclerotic therapy. Mol Pharm. 2019;16:3284–91.
41. Nagy A, Zane A, Cole SL, Severance M, Dutta PK, Waldman WJ. Contrast of the biological activity of negatively and positively charged microwave synthesized CdSe/ZnS quantum Dots. Chem Res Toxicol. 2011;24:2176–88.
42. Ekkelenkamp AE, Jansman MMT, Roelofs K, Engbersen JFJ, Paulusse JMJ. Surfactant-free Preparation of highly stable zwitterionic poly(amido amine) nanogels with minimal cytotoxicity. Acta Biomater. 2016;30:126–34.
43. Song X, Fischer P, Chen X, Burton C, Wang J. An apoA-I mimetic peptide facilitates off-loading cholesterol from HDL to liver cells through scavenger receptor BI. Int J Biol Sci. 2009;5:637–46.
44. Liu Q, Wang Y-M, Gu H-F. Lipophagy in atherosclerosis. Clin Chim Acta. 2020;511:208–14.
45. Geng M-Y, Wang L, Song Y-Y, Gu J, Hu X, Yuan C, Yang M, Pei W-J, Zhang Y, Gao J-L. Sidt2 is a key protein in the autophagy-lysosomal degradation pathway and is essential for the maintenance of kidney structure and filtration function. Cell Death Dis. 2021;13:7.
46. Wang X, Wang C, Tian H, Chen Y, Wu B, Cheng W. IR-820@NBs combined with MG-132 enhances the Anti-Hepatocellular carcinoma effect of sonodynamic therapy. Int J Nanomed. 2023;18:6199–212.
47. Zhao J, Hu B, Xiao H, Yang Q, Cao Q, Li X, Zhang Q, Ji A, Song S. Fucoidan reduces lipid accumulation by promoting foam cell autophagy via TFEB. Carbohydr Polym. 2021;268:118247.
48. Cruz ALS, Carrossini N, Teixeira LK, Ribeiro-Pinto LF, Bozza PT, Viola JPB. Cell cycle progression regulates biogenesis and cellular localization of lipid droplets. Mol Cell Biol. 2019;39:e00374–18.
49. Mathiassen SG, De Zio D, Cecconi F. Autophagy and the cell cycle: A complex landscape. Front Oncol. 2017;7:51.
50. Gschwind A, Marx C, Just MD, Severin P, Behring H, Marx-Blümel L, Becker S, Rothenburger L, Förster M, Beck JF, et al. Tight association of autophagy and cell cycle in leukemia cells. Cell Mol Biol Lett. 2022;27:32.
51. Morimoto Y, Saitoh S, Takayama Y. Growth conditions inducing G1 cell cycle arrest enhance lipid production in the oleaginous yeast lipomyces starkeyi. J Cell Sci. 2022;135:jcs259996.
52. Wu H, Ploeger JM, Kamarajugadda S, Mashek DG, Mashek MT, Manivel JC, Shekels LL, Lapiro JL, Albrecht JH. Evidence for a novel regulatory interaction involving Cyclin D1, lipid droplets, lipolysis, and cell cycle progression in hepatocytes. Hepatol Commun. 2019;3:406–22.
53. Wang X, Li L, Niu X, Dang X, Li P, Qu L, Bi X, Gao Y, Hu Y, Li M, et al. mTOR enhances foam cell formation by suppressing the autophagy pathway. DNA Cell Biol. 2014;33:198–204.
54. Day EA, Ford RJ, Steinberg GR. AMPK as a therapeutic target for treating metabolic diseases. Trends Endocrinol Metab. 2017;28:545–60.
55. Ou H, Liu C, Feng W, Xiao X, Tang S, Mo Z. Role of AMPK in atherosclerosis via autophagy regulation. Sci China Life Sci. 2018;61:1212–21.
56. Qiao L, Zhang X, Liu M, Liu X, Dong M, Cheng J, Zhang X, Zhai C, Song Y, Lu H, et al. Ginsenoside Rb1 enhances atherosclerotic plaque stability by improving autophagy and lipid metabolism in macrophage foam cells. Front Pharmacol. 2017;8:727.
57. Varshney R, Varshney R, Mishra R, Gupta S, Sircar D, Roy P. Kaempferol alleviates palmitic acid-induced lipid stores, Endoplasmic reticulum stress and pancreatic β-cell dysfunction through AMPK/mTOR-mediated lipophagy. J Nutr Biochem. 2018;57:212–27.
58. Yoo J, Jeong I-K, Ahn KJ, Chung HY, Hwang Y-C. Fenofibrate, a PPARα agonist, reduces hepatic fat accumulation through the upregulation of TFEB-mediated lipophagy. Metabolism. 2021;120:154798.
59. Wei C-C, Luo Z, Hogstrand C, Xu Y-H, Wu L-X, Chen G-H, Pan Y-X, Song Y-F. Zinc reduces hepatic lipid deposition and activates lipophagy via Zn2+/MTF-1/PPARα and Ca2+/CaMKKβ/AMPK pathways. FASEB J 2018;fj201800463. Online ahead of print.
60. Ren T, Tang Y-J, Wang M-F, Wang H-S, Liu Y, Qian X, Chang C, Chen M-W. Triptolide induces apoptosis through the calcium/calmodulin–dependent protein kinase kinaseβ/AMP–activated protein kinase signaling pathway in non–small cell lung cancer cells. Oncol Rep. 2020;44:2288–96.
61. Chen J, Li L, Li Y, Liang X, Sun Q, Yu H, Zhong J, Ni Y, Chen J, Zhao Z, et al. Activation of TRPV1 channel by dietary capsaicin improves visceral fat remodeling through connexin43-mediated Ca2 + influx. Cardiovasc Diabetol. 2015;14:22.
62. Xin S, Mueller C, Pfeiffer S, Kraft VAN, Merl-Pham J, Bao X, Feederle R, Jin X, Hauck SM, Schmitt-Kopplin P, et al. MS4A15 drives ferroptosis resistance through calcium-restricted lipid remodeling. Cell Death Differ. 2022;29:670–86.
63. Chauhan AS, Liu X, Jing J, Lee H, Yadav RK, Liu J, Zhou Y, Gan B. STIM2 interacts with AMPK and regulates calcium-induced AMPK activation. FASEB J. 2019;33:2957–70.
64. Yuan W, Fang W, Zhang R, Lyu H, Xiao S, Guo D, Ali DW, Michalak M, Chen X-Z, Zhou C, et al. Therapeutic strategies targeting AMPK-dependent autophagy in cancer cells. Biochim Biophys Acta Mol Cell Res. 2023;1870:119537.
65. Liu T-Y, Xiong X-Q, Ren X-S, Zhao M-X, Shi C-X, Wang J-J, Zhou Y-B, Zhang F, Han Y, Gao X-Y, et al. FNDC5 alleviates hepatosteatosis by restoring AMPK/mTOR-Mediated autophagy, fatty acid oxidation, and lipogenesis in mice. Diabetes. 2016;65:3262–75.
66. Wong VKW, Qiu C, Xu S-W, Law BYK, Zeng W, Wang H, Michelangeli F, Dias IRDSR, Qu YQ, Chan TW, et al. Ca2 + signalling plays a role in celastrol-mediated suppression of synovial fibroblasts of rheumatoid arthritis patients and experimental arthritis in rats. Br J Pharmacol. 2019;176:2922–44.
67. Pham TH, Lee GH, Jin SW, Lee SY, Han EH, Kim ND, Choi CY, Jeong G-S, Ki Lee S, Kim HS, et al. Sesamin ameliorates lipotoxicity and lipid accumulation through the activation of the Estrogen receptor alpha signaling pathway. Biochem Pharmacol. 2023;216:115768.
68. Laval T, Ouimet M. A role for lipophagy in atherosclerosis. Nat Rev Cardiol. 2023;20:431–2.
69. Diao Y, Clematichinenoside AR. Alleviates foam cell formation and the inflammatory response in Ox-LDL-Induced RAW264.7 cells by activating autophagy. Inflammation. 2021;44:758–68.
70. Ouimet M, Marcel YL. Regulation of lipid droplet cholesterol efflux from macrophage foam cells. Arterioscler Thromb Vasc Biol. 2012;32:575–81.
71. Xu H, Zhao H, Ding C, Jiang D, Zhao Z, Li Y, Ding X, Gao J, Zhou H, Luo C, et al. Celastrol suppresses colorectal cancer via covalent targeting Peroxiredoxin 1. Signal Transduct Target Ther. 2023;8:51.
72. Wagh PR, Desai P, Prabhu S, Wang J. Nanotechnology-Based Celastrol formulations and their therapeutic applications. Front Pharmacol. 2021;12:673209.
73. Wang B, Tang X, Yao L, Wang Y, Chen Z, Li M, Wu N, Wu D, Dai X, Jiang H, et al. Disruption of USP9X in macrophages promotes foam cell formation and atherosclerosis. J Clin Invest. 2022;132:e154217.
74. Luo H, Wang J, Qiao C, Ma N, Liu D, Zhang W. Pycnogenol attenuates atherosclerosis by regulating lipid metabolism through the TLR4-NF-κB pathway. Exp Mol Med. 2015;47:e191.
75. Gu L, Bai W, Li S, Zhang Y, Han Y, Gu Y, Meng G, Xie L, Wang J, Xiao Y, et al. Celastrol prevents atherosclerosis via inhibiting LOX-1 and oxidative stress. PLoS ONE. 2013;8:e65477.
76. Shi Y-N, Liu L-P, Deng C-F, Zhao T-J, Shi Z, Yan J-Y, Gong Y-Z, Liao D-F, Qin L. Celastrol ameliorates vascular neointimal hyperplasia through Wnt5a-involved autophagy. Int J Biol Sci. 2021;17:2561–75.
77. Fan N, Zhao J, Zhao W, Zhang X, Song Q, Shen Y, Shum HC, Wang Y, Rong J. Celastrol-loaded lactosylated albumin nanoparticles attenuate hepatic steatosis in non-alcoholic fatty liver disease. J Control Release. 2022;347:44–54.
78. Xie Q, Zhao S, Li F. D-4F, an Apolipoprotein A-I mimetic peptide, promotes cholesterol efflux from macrophages via ATP-binding cassette transporter A1. Tohoku J Exp Med. 2010;220:223–8.
79. Lin H-P, Singla B, Ahn W, Ghoshal P, Blahove M, Cherian-Shaw M, Chen A, Haller A, Hui DY, Dong K, et al. Receptor-independent fluid-phase

macropinocytosis promotes arterial foam cell formation and atherosclerosis. Sci Transl Med. 2022;14:eadd2376.
80. Zhou M, Ren P, Zhang Y, Li S, Li M, Li P, Shang J, Liu W, Liu H. Shen-Yuan-Dan capsule attenuates atherosclerosis and foam cell formation by enhancing autophagy and inhibiting the PI3K/Akt/mTORC1 signaling pathway. Front Pharmacol. 2019;10:603.
81. Tang Y, Wu H, Shao B, Wang Y, Liu C, Guo M. Celosins inhibit atherosclerosis in ApoE-/- mice and promote autophagy flow. J Ethnopharmacol. 2018;215:74–82.
82. Shi Y, Jiang S, Zhao T, Gong Y, Liao D, Qin L. Celastrol suppresses lipid accumulation through LXRα/ABCA1 signaling pathway and autophagy in vascular smooth muscle cells. Biochem Biophys Res Commun. 2020;532:466–74.
83. Ma A, Wang J, Yang L, An Y, Zhu H. AMPK activation enhances the anti-atherogenic effects of high density lipoproteins in apoE-/- mice. J Lipid Res. 2017;58:1536–47.
84. Chen M, Zhu J-Y, Mu W-J, Luo H-Y, Li Y, Li S, Yan L-J, Li R-Y, Guo L. Cdo1-Camkk2-AMPK axis confers the protective effects of exercise against NAFLD in mice. Nat Commun. 2023;14:8391.
85. Li J, Wang X, Meng X, Zhou X, Huang H, Feng Y, Fu Y, Liu X, Yu B. Geraniin targeting CaMKK2 inhibits lipid accumulation in 3T3-L1 adipocytes by suppressing lipogenesis. Chem Biol Interact. 2023;372:110364.
86. Wang S, Yi X, Wu Z, Guo S, Dai W, Wang H, Shi Q, Zeng K, Guo W, Li C. CAMKK2 defines ferroptosis sensitivity of melanoma cells by regulating AMPK–NRF2 pathway. J Invest Dermatol. 2022;142:189–e2008.
87. Giordano A, Murano I, Mondini E, Perugini J, Smorlesi A, Severi I, Barazzoni R, Scherer PE, Cinti S. Obese adipocytes show ultrastructural features of stressed cells and die of pyroptosis. J Lipid Res. 2013;54:2423–36.
88. Arruda AP, Hotamisligil GS. Calcium homeostasis and organelle function in the pathogenesis of obesity and diabetes. Cell Metab. 2015;22:381–97.
89. Bi J, Wang W, Liu Z, Huang X, Jiang Q, Liu G, Wang Y, Huang X. Seipin promotes adipose tissue fat storage through the ER Ca^{2+}-ATPase SERCA. Cell Metab. 2014;19:861–71.
90. Shi W, Xu D, Gu J, Xue C, Yang B, Fu L, Song S, Liu D, Zhou W, Lv J, et al. Saikosaponin-d inhibits proliferation by up-regulating autophagy via the CaMKKβ-AMPK-mTOR pathway in ADPKD cells. Mol Cell Biochem. 2018;449:219–26.
91. Masuda M, Yoshida-Shimizu R, Mori Y, Ohnishi K, Adachi Y, Sakai M, Kabutoya S, Ohminami H, Yamanaka-Okumura H, Yamamoto H, et al. Sulforaphane induces lipophagy through the activation of AMPK-mTOR-ULK1 pathway signaling in adipocytes. J Nutr Biochem. 2022;106:109017.

Publisher's note